

# Policies for multiplexed quantum repeaters: theory and practical performance analysis

Stav Haldar,<sup>1,\*</sup> Pratik J. Barge,<sup>1,†</sup> Xiang Cheng,<sup>2,‡</sup> Kai-Chi Chang,<sup>2,§</sup>  
Brian T. Kirby,<sup>3,4,¶</sup> Sumeet Khatri,<sup>5,\*\*</sup> Chee Wei Wong,<sup>2,††</sup> and Hwang Lee<sup>1,‡‡</sup>

<sup>1</sup>*Hearne Institute for Theoretical Physics, Department of Physics and Astronomy,  
Louisiana State University, Baton Rouge, Louisiana 70803, USA*

<sup>2</sup>*Fang Lu Mesoscopic Optics and Quantum Electronics Laboratory,  
Department of Electrical and Computer Engineering,  
University of California, Los Angeles, California 90095, USA*

<sup>3</sup>*DEVCOM Army Research Laboratory, Adelphi, MD 20783, USA*

<sup>4</sup>*Tulane University, New Orleans, LA 70118, USA*

<sup>5</sup>*Dahlem Center for Complex Quantum Systems, Freie Universität Berlin, 14195 Berlin, Germany*  
(Dated: January 25, 2024)

Future quantum networks will have nodes equipped with multiple quantum memories, providing the possibility to perform multiplexing and distillation strategies in order to increase fidelities and reduce waiting times for end-to-end entanglement distribution. In this paper, we introduce two policies that adapt the well-known swap-as-soon-as-possible (SWAP-ASAP) policy to multiplexed quantum repeater chains. Unlike the usual, fully local SWAP-ASAP policy, these policies are “quasi-local”, making effective use of knowledge of the states of the repeaters along the chain to optimize waiting times and end-to-end fidelities. Our policies also make use of entanglement distillation. We demonstrate via simulations one of our key findings, which is that these policies can outperform the well-known and widely studied nested purification and doubling swapping policy in practically relevant parameter regimes. Our work also provides the tools to carefully examine the role of entanglement distillation. We identify the parameter regimes in which performing distillation makes sense and is useful. In these regimes, we also address the question: “*Should we distill before swapping, or vice versa?*” We thus formalize the trade-off between the advantages of adding distillation capabilities to quantum networks against their technological and practical challenges. Finally, to provide further practical guidance, we propose an experimental implementation of a multiplexing-based linear network, and experimentally demonstrate the key element, a high-dimensional biphoton frequency comb (BFC). We then evaluate the anticipated performance of our multiplexing-based policies in such a real-world network through simulation results for two concrete memory platforms, namely rare-earth ions and diamond vacancies.

## I. INTRODUCTION

The quantum internet [1–3] has the potential to revolutionize current computation, communication, and sensing technologies by enabling exchange of quantum data. Numerous significant applications have already been recognized, encompassing areas such as secure quantum communication [4, 5], distributed quantum computation [6, 7], and distributed quantum sensing [8–10], to name a few. However, enormous hardware improvements are needed before a practical quantum internet is realized [11, 12]. Currently, a significant challenge lies in effectively distributing entanglement amongst network nodes, particularly over significant distances. Recent, state-of-the-art experiments have been performed for only a handful of nodes over short distances [13, 14]. This challenge stems from the delicate nature of quantum systems, leading to issues like photon losses, imperfect measurements, and quantum memories with short coherence times. Since comprehensive, fault-tolerant

quantum error correction has yet to be realized to overcome these obstacles, it becomes important to explore how much we can overcome these limitations through other means. This problem of designing effective protocols for entanglement distribution using noisy, imperfect quantum hardware has been addressed in multiple analytical [15–33] and numerical [34–43] studies, among others; see also Refs. [44–50] for reviews.

In the context of entanglement distribution in quantum repeater chains, the “single-channel” approach has been commonly studied. In the single-channel setting, every repeater is connected via a single channel to each of its two neighbors, with a single quantum memory at the endpoint of each channel. These channels are used to create elementary links of entangled qubit pairs between the neighboring nodes. Then, using a particular policy for performing probabilistic entanglement-swapping operations [51, 52], the elementary links are transformed into a virtual link between the two end nodes of the repeater chain, which can be further used for exchanging quantum information via the quantum teleportation protocol [51]. Noise and loss along the channels, along with quantum memories with short coherence times, result in long waiting times and/or low fidelities of the end-to-end entangled links.

In this work, we look at the multiplexing approach [17] as a potential method for reducing the overall waiting time for entanglement generation in linear networks and increasing the fidelity of end-to-end entangled links; see Fig. 1. In a multiplexing protocol, every repeater contains multiple memories, which are connected by multiple channels, as shown in

\* hstav1@lsu.edu

† pbarge1@lsu.edu

‡ chengxiang@ucla.edu

§ uclakcchang@g.ucla.edu

¶ brian.t.kirby4.civ@army.mil

\*\* sumeet.khatri@fu-berlin.de

†† cheewei.wong@ucla.edu

‡‡ hwlee@lsu.edu

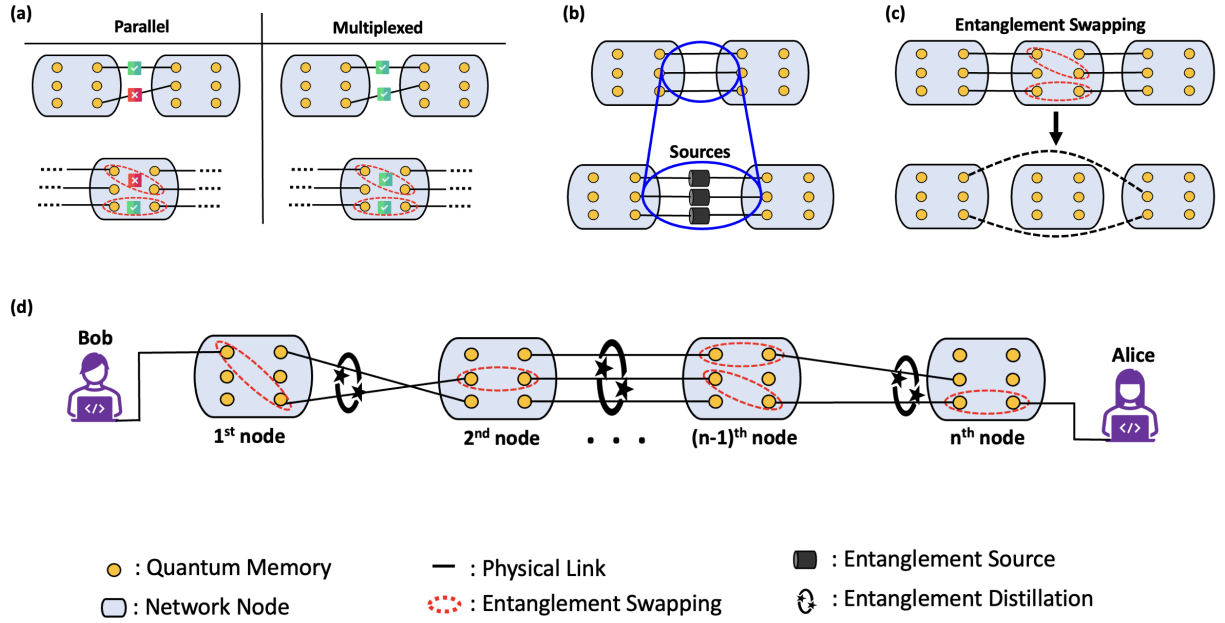


FIG. 1. (a) Difference between the parallel and multiplexing approaches. Unlike the parallel approach, cross-channel elementary link generation and entanglement swapping is permitted in the multiplexing approach. (b) Elementary links are created by multiple entanglement generation sources associated with every channel that connects different pairs of quantum memories. (c) Non-neighbouring nodes are connected by virtual links generated by performing entanglement swapping operations between neighbouring active quantum memories. (d) Linear chain of quantum repeaters with multiple quantum memories capable of establishing multiple physical links, entanglement distillation and entanglement swapping.

Fig. 1(a). This allows for simultaneous elementary link generation attempts. Furthermore, when performing entanglement swapping, it is possible to go beyond the trivial parallel approach and perform cross-channel entanglement swapping; see Fig. 1(a). There is also the possibility to perform entanglement purification/distillation [53–56].

Despite the significant benefits of approaches based on multiplexing and/or distillation already studied and demonstrated in the literature [15, 16, 57–74], many open questions remain in terms of efficient and optimal entanglement swapping and distillation policies for linear quantum repeater chains. In particular, many of the aforementioned works on multi-memory quantum repeaters with multiplexing have made use of the “nested purification and doubling swapping” protocol devised in the seminal works [15, 16] on quantum repeaters. We therefore ask the following two questions.

1. Is the nested purification and doubling swapping policy optimal, particularly in the practically-relevant parameter regimes of low coherence times and low elementary link success probabilities?
2. What is the best way to combine entanglement swapping with entanglement distillation? Should we distill first before swapping, or vice versa?

### A. Overview of results

In this work, we start by extending the framework from Ref. [43] for modeling quantum repeater chains in terms of

Markov decision processes to the case of multi-memory quantum repeater chains (see Sec. II). Then, we use this model to address the two questions above.

Our main results and contributions comprise four parts.

#### 1. New policies for multiplexed quantum repeaters.

In Sec. III, we define our multiplexing-based policies. These policies are generalizations of the so-called “swap-as-soon-as-possible” (SWAP-ASAP) policy [29, 30] to the multiplexing setting. We refer to them as *strongest neighbor* (SN) SWAP-ASAP, *farthest neighbor* (FN) SWAP-ASAP, and *random* SWAP-ASAP. These policies are distinguished by how they pair memories within nodes for the purposes of entanglement swapping. Intuitively, the SN SWAP-ASAP policy prioritizes the creation of high-fidelity end-to-end links, and FN SWAP-ASAP prioritizes lowering the waiting time for the creation of end-to-end links. These policies are also “quasi-local”, requiring some knowledge of the network state but not full, global knowledge.

In Sec. IV, we compare the performance of these policies and show that the SN, FN, and random SWAP-ASAP policies can significantly reduce the average waiting time compared to the parallel, non-multiplexed version of SWAP-ASAP, and at the same time provide higher end-to-end link fidelities.

Notably, the SN and FN policies can outperform the widely used doubling protocol for entanglement swapping in certain parameter regimes. More specifically, in Sec. IV A, we see improved performance of our policies in more resource-constrained scenarios, such as high

channel losses, high qubit noise (small coherence time of quantum memories), and when the number of multiplexing channels is small and/or the number of network nodes is large. These parameter regimes are relevant for near-term quantum network implementations.

## 2. Policies with entanglement distillation.

Then, in Sec. V, we add distillation to our FN and SN SWAP-ASAP policies, and we address the following questions: i) “When is distillation useful?” ii) “Should we distill before swapping, or swap first and then distill?” We demonstrate via simulations that these policy considerations have a strong influence on the performance of the network. As such, with our study, we provide the tools to weigh the technological and practical challenges of adding distillation abilities to quantum networks against the advantages of adding such an ability.

## 3. The impact of classical communication costs.

In Sec. VI, we consider the classical communication (CC) costs associated with our policies. By incorporating the time needed for CC into our model, we show that our multiplexing-based FN and SN SWAP-ASAP policies outperform fully-local policies that do not require any CC. We thus show that the benefit gained by acquiring information about the network’s state is retained even when the communication costs of acquiring such information is accounted for. This result provides much needed evidence in support of exploring policies that use knowledge of the network state, as promoted in previous literature [41–43]. We also show that, even when CC costs are accounted for, the FN and SN SWAP-ASAP policies can outperform the doubling policy in parameter regimes corresponding to resource-constrained hardware settings.

## 4. Design and analysis of real-world repeater chains.

In Sec. VII, we outline a proof-of-principle experimental realization of a quantum network equipped with multiplexing policies using a high-dimensional bi-photon frequency comb (BFC), and we map the relevant experimental parameters to their counterpart parameters within our modeling framework. Then, in Sec. VII B, we assess the performance of our multiplexing-based policies within these parameter regimes for two quantum memory platforms, diamond vacancy and rare-earth metal ions.

## II. LINEAR CHAIN QUANTUM NETWORK WITH MULTIPLE CHANNELS

Throughout this work, we consider entanglement distribution in a linear chain network of quantum repeaters. In this section, we present our theoretical model for entanglement distribution in such networks; see also Fig. 1.

- *Nodes:* The linear chain is made up of  $n$  nodes. Every node contains multiple quantum memories. Specifically,

every node has  $2n_{ch}$  quantum memories. Given the linear nature of our networks,  $n_{ch} \in \{1, 2, \dots\}$  corresponds to the number of channels connecting the nearest-neighbor nodes. (In Fig. 1,  $n_{ch} = 3$ .) Every memory has a finite coherence time of  $m^* \in \{0, 1, \dots\}$  time steps, which specifies the maximum number of (discrete) time steps that qubits can be stored in the memory.

- *Elementary and virtual links:* Entanglement sources establish physical/elementary links between nearest-neighbour quantum memories with probability  $p_\ell \in [0, 1]$ . A probabilistic Bell state measurement creates a virtual link between distant quantum memories with success probability  $p_{sw} \in [0, 1]$ . These values are fundamentally limited by the technology used to create the system, e.g., linear optics makes  $p_{sw} \leq 0.5$ , and  $p_\ell$  is determined by properties of the source, loss characteristics of the sources, etc. These considerations are relevant for our proposed experimental implementation in Sec. VII, and we provide details on how to determine  $p_\ell$  and  $m^*$  from physical properties of the system in Sec. VII A.

We keep track of the fidelity of both elementary and virtual links by assigning every link an age. The age  $m$  of a link starts from  $m = m_0$ , when it is first created, with  $m_0$  being a measure of its initial fidelity with respect to a perfect Bell state. The age then increases in discrete steps, such that  $m \in \{0, 1, 2, 3, \dots\}$ . Once the age of the link reaches  $m^*$ , the link is discarded. Throughout this work, we consider a particular Pauli noise model for decoherence of the memories (see Appendix A), such that the fidelity  $f(m)$  of a link that has age  $m$  is given by

$$f(m) = \frac{1}{4}(1 + 3e^{-\frac{m}{m^*}}). \quad (1)$$

The age of a link formed by a successful entanglement swapping operation is determined by adding the ages of the two corresponding links: if  $m_1$  and  $m_2$  are the ages of the two links, then if the entanglement swapping is successful the age of the new link is  $m' = m_1 + m_2$ . This “addition rule” for the age of virtual links is a direct consequence of the Pauli noise model that we use, and a proof can be found in Ref. [43, Appendix C].

- *Entanglement distillation:* Multiple low-fidelity links between any two nodes can be distilled with probability  $p_{ds} \in [0, 1]$  to form a higher-fidelity link. Throughout this work, we consider the BBPSSW protocol [53], and we provide details on it in Appendix B.

Entanglement distribution protocols progress in a series of discrete time steps, based on the Markov decision process model developed and used in Ref. [43], which we refer to for further details on the model. In every time step, the following events occur.

1. Check the number of active links to the right of every node (except for the right-most node). If there are inactive links, request the corresponding elementary link.

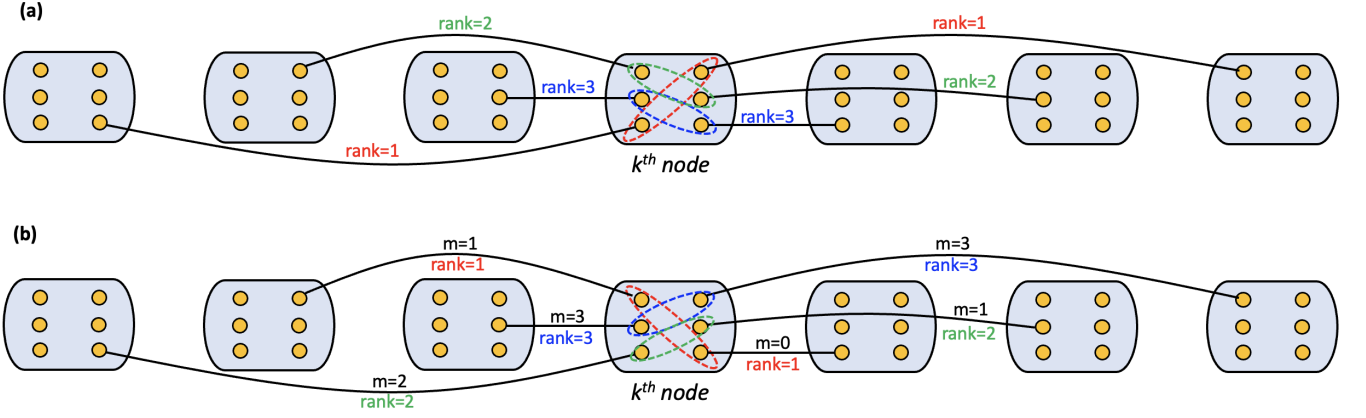


FIG. 2. (a) Illustrative example of the FN SWAP-ASAP policy. Links on both sides of the  $k^{\text{th}}$  node are ranked separately on the basis of their lengths. The longest link is given a rank of 1, while shortest is ranked 3. For entanglement swapping, we thus give first preference to links of rank 1 (marked in red), which would result in the longest possible link. Being a probabilistic process, if the entanglement swapping fails, then next preferences is given to links of rank 2, and so on. (b) In the case of the SN SWAP-ASAP policy, link rankings are based on their ages. Preference is given to links with lower ages.

2. Check the number of active links to the left and right of every node, except for the end nodes. If more than one link on either side is active, rank them based on the policy, as described in detail in Sec. III below. If the doubling policy is being used, pair the links for entanglement swapping only if they are the same length. Perform the entanglement swapping operations in the ranked order. Entanglement swapping is attempted only if the sum of the ages of the two links is less than  $m^*$ .
3. If entanglement distillation is part of the policy, attempt to distill all links between the same two nodes for a given number of rounds, as dictated by the policy; see Sec. V for details. If the policy calls for distilling first, then swapping, interchange steps 2 and 3.
4. Increase the age of all active links by one time unit, accounting for decoherence. If classical communication (CC) overheads are to be accounted for, then add the CC time to the age of every active link; see Sec. VI for details. Discard any link which has age greater than  $m^*$ .

### III. POLICIES FOR MULTIPLEXING

In this section, we introduce our two multiplexing policies for entanglement distribution in a linear chain quantum network.

When multiple links are available between nodes of the network, there are many possibilities for how to perform entanglement swapping. There is also the possibility to perform entanglement distillation between nodes that share several links. In linear quantum networks without multiplexing (i.e.,  $n_{ch} = 1$  in Fig. 1), one of the simplest and best studied swapping protocols is swap-as-soon-as-possible (SWAP-ASAP). As the name suggests, the SWAP-ASAP policy dictates that entanglement swapping should be attempted as soon as two memories in a given node become active, i.e., as soon as an entanglement swapping

policy becomes possible. SWAP-ASAP policies have been shown to be better than fixed nesting or doubling policies for a large set of parameter regimes in linear chain networks consisting of a single channel between nodes [25, 30, 75]. The policies we present in this work are generalizations of the SWAP-ASAP policy to the multiplexing setting.

The direct application of SWAP-ASAP in multiplexed linear chains is unspecified due to the increased degrees of freedom. In particular, two immediate questions arise:

1. If the opportunity is available simultaneously, should we preferably perform entanglement swapping on links that result in a virtual link between *farthest* nodes or the ones that result in a *strongest*—highest fidelity—virtual link? Based on this question, we define the following two generalizations of SWAP-ASAP for multiplexed linear chains.
  - (a) The *Farthest Neighbor (FN) SWAP-ASAP policy*: This policy prioritizes the creation of virtual links between faraway nodes. Accordingly, we rank the links based on their lengths (farthest links are ranked first), and then entanglement swapping is performed in that order. This policy is illustrated with an example in Fig. 2.
  - (b) The *Strongest Neighbor (SN) SWAP-ASAP policy*: This policy prioritizes the creation of virtual links with high fidelity. Accordingly, we rank the links based on their ages (links with the lowest age are ranked first), and then entanglement swapping is performed in that order.

For comparison, we also define the *random SWAP-ASAP* policy. In the random SWAP-ASAP policy, links are randomly paired to perform entanglement swapping operations, without any consideration of their length and/or age. We also define the *parallel SWAP-ASAP* to be the non-multiplexed version of the usual SWAP-ASAP policy.



2. What should be the preference when it comes to the order of entanglement distillation and swapping—should we distill first and then swap, or the other way around? We call these two distinct options the **DISTILL-SWAP** and **SWAP-DISTILL** policies. Both of these may be used in conjunction with the SN and FN entanglement swapping policies defined above, leading to four distinct policy combinations.

The motivation behind our definitions of the FN and SN **SWAP-ASAP** policies is based on prior works [41–43], which have shown that policies that make use of global knowledge of the state of the repeater chain offer an advantage in terms of waiting time and fidelity. At the same time, such global knowledge comes with considerable classical communication cost and hence is not practical for networks with a large number of nodes and long link distances. This limitation motivated the proposal of so-called *quasi-local* policies in Ref. [43], which are policies that use global knowledge and coordination between small groups of nodes, but still use local policies such as **SWAP-ASAP** to connect such groups to each other. The SN and FN **SWAP-ASAP** policies being defined here are also quasi-local policies: the nodes do not have knowledge of the entire network, but they have information about other nodes they are connected to. We stress here that access to such information comes with classical communication (CC) costs, but such costs will be much smaller than fully global policies, in which each node knows about the state of every other network node at all times. More precisely, for fully global policies the CC cost in each time step will be proportional to the communication time from one end of the network to another. This would place considerable demands on the coherence times of quantum memories used in the network. On the other extreme, for fully-local policies all CC can be deferred to one round of end-to-end communication at the end of the entanglement distribution protocol. Quasi-local policies try to find a middle ground between these extremes.

Throughout the rest of this work, we demonstrate via simulations that our quasi-local SN and FN **SWAP-ASAP** multiplexing policies can outperform (in terms of waiting time and end-to-end fidelity) not only non-multiplexed or parallel policies but also fully-local multiplexed policies in which decisions about entanglement swapping are made without utilising any knowledge of the network’s state,

like in the *random* multiplexing policy. We also demonstrate via simulations that our policies can outperform the well-known and widely-used doubling and nested-purification-and-swapping protocol.

Before proceeding, we remark that very recently in Ref. [76], the idea of using fidelity-based ranks to match links for entanglement swapping (similar in spirit to our SN **SWAP-ASAP** policy) was proposed, but the focus was on second-generation repeaters with error-correction capabilities. Our focus here is on first-generation repeaters. See Refs. [77, 78] for the definitions of first- and second-generation quantum repeaters.

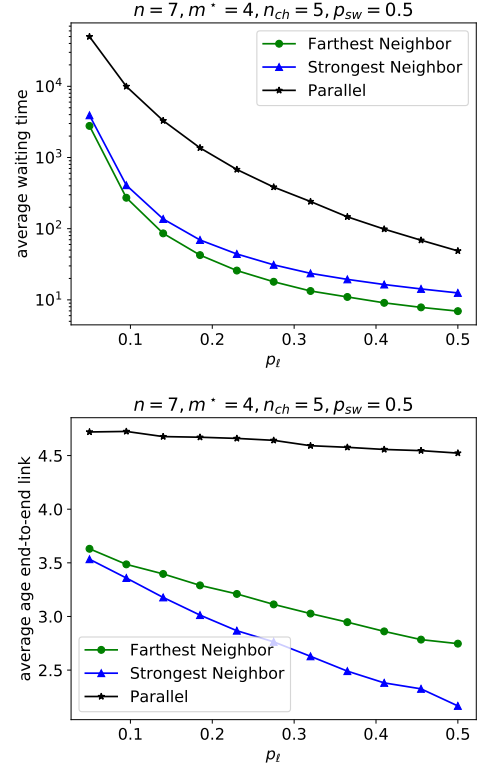


FIG. 3. Average waiting time and average age of the youngest end-to-end link for a repeater chain with  $n = 7$  nodes, according to the multiplexed (SN and FN **SWAP-ASAP**) and non-multiplexed (parallel **SWAP-ASAP**) policies. The multiplexed versions can enormously reduce average waiting time compared to parallel **SWAP-ASAP**, and at the same time increase end-to-end link fidelities. SN is the better choice for fidelity enhancement, while FN reduces the waiting time more significantly.

#### IV. PERFORMANCE OF MULTIPLEXING BASED POLICIES

Having defined our SN and FN **SWAP-ASAP** policies in the previous section, we now evaluate their performance. We consider two figures of merit: the average waiting time and the average age of the youngest end-to-end link. In this section, we measure the average waiting time in terms of the number of time steps. This unitless, abstract quantity can be converted into physical times, and also the ages converted to fidelity values, by incorporating the network hardware and design parameters. Examples of such a translation are given in Sec. IV and further details are provided in Sec. VII A and Appendix A.

Intuitively, based on their definitions, the FN **SWAP-ASAP** policy aims to create the longest possible links, with the aim of creating an end-to-end link in the smallest possible number of time steps. Thus, the FN **SWAP-ASAP** policy qualitatively prioritizes minimizing the average waiting time. On the other hand, the SN **SWAP-ASAP** policy aims to create the strongest or highest-fidelity links between the end nodes of the network. In order to confirm this intuitive picture, and to ascertain the benefit of multiplexing with these two policies, we benchmark the FN

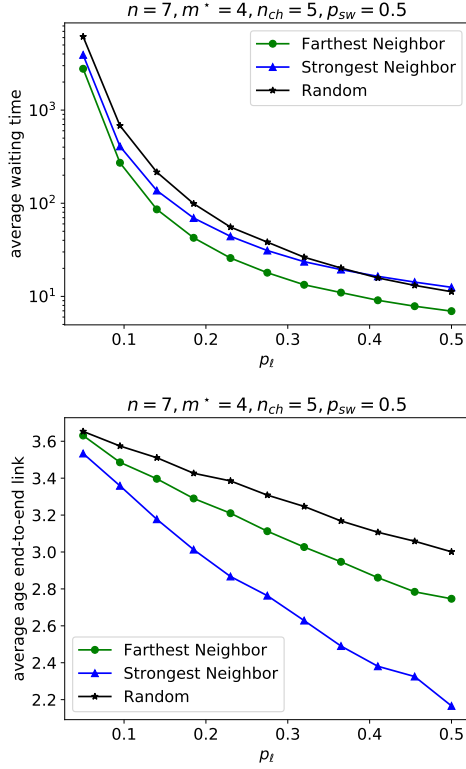


FIG. 4. Average waiting time and average age of the youngest end-to-end link for a repeater chain with  $n = 7$  nodes, according to the FN, SN, and random SWAP-ASAP multiplexing policies. SN and FN both outperform the random policy, indicating the benefit of using knowledge of the network state. SN is the better choice for fidelity enhancement, while FN reduces the waiting time more significantly.

and SN policies against  $n_{ch}$  copies of the usual SWAP-ASAP run in *parallel*. In Fig. 3, we show that the multiplexed versions can indeed, as expected, enormously reduce the average waiting time compared to the parallel version of SWAP-ASAP, and at the same time provide higher end-to-end fidelities.

In Fig. 3, and for all of the plots shown in this paper, the parameter values that we choose are based on what is computationally feasible, but they are also based on what we expect with actual hardware, as we outline in Sec. VII A. The choice of network parameters such as  $p_\ell$ ,  $m^*$  etc. in specific examples is also motivated by the intent to show the most prominent and overarching trends.

The advantage of our SN and FN policies is not only based on the trivial advantage one would expect by shifting from a parallel policy to a multiplexing policy. Even amongst multiplexing policies, the SN and FN policies can be advantageous. Indeed, the fact that we assign ranks to different links and use this knowledge to perform entanglement swapping also provides considerable advantage. To show this advantage, we compare SN and FN multiplexing policies against the random SWAP-ASAP multiplexing policy defined above. As expected, both SN and FN policies perform better than the random policy, as we show in Fig. 4. We also see that the FN policy provides lower average waiting times compared to the SN policy, and the SN policy

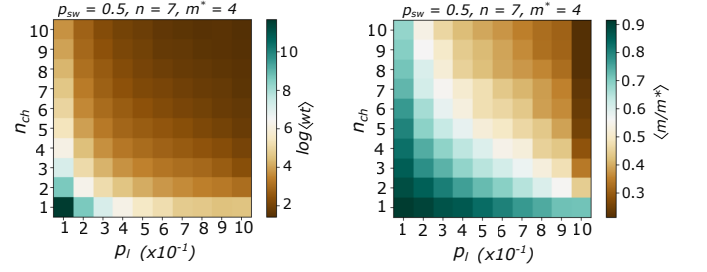


FIG. 5. Heat map of average waiting time (left) (denoted  $\langle wt \rangle$ ) and ratio of the average age of youngest end-to-end link to the cutoff (right) as a function of elementary link success probability and number of channels. Contours of fixed values run along diagonals from the top-left to the bottom-right, showing that lower link probabilities can be compensated for by increasing the number of channels. Both the average waiting time and the average age of the youngest end-to-end link reduce as the number of channels increases, showing the usefulness of multiplexing. For the waiting time results we use the FN policy, and for the average age results we use the SN policy.

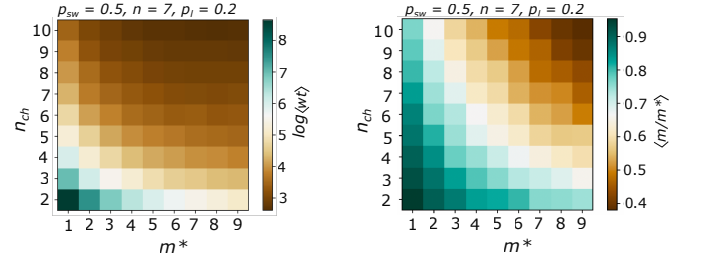


FIG. 6. Heat map of average waiting time (left) (denoted by  $\langle wt \rangle$ ) and ratio of the average age of youngest end-to-end link to the cutoff (right) as a function of link cutoff age and number of channels. Contours of fixed values run along diagonals from the top-left to the bottom-right, showing that lower cutoffs, which translates to memories with smaller coherence times, can be compensated for by increasing the number of channels. For waiting time results we use the FN policy and for average age results we use SN policy.

provides a higher-fidelity end-to-end link compared to the FN policy, verifying our intuition.

Next, we look at how increasing the number  $n_{ch}$  of channels affects the average waiting time of the repeater chain. Increasing  $n_{ch}$  increases the effective  $p_\ell$  of the chain according to  $p_\ell \rightarrow 1 - (1 - p_\ell)^{n_{ch}}$ ; therefore, in Fig. 5, approximately constant values of the waiting time run along the diagonal from the top-left to the bottom-right, indicating that as the elementary link probability goes down, in order to keep the average waiting time and end-to-end fidelity constant, we should increase the number of channels. In other words, for a given average waiting time or end-to-end fidelity requirement, low elementary link probabilities can be compensated for by increasing the number of multiplexing channels.

In Fig. 6, we fix the elementary link and entanglement swapping success probabilities while varying  $n_{ch}$  and the coherence time  $m^*$ . Here we see a similar trend, a low value of the memory coherence time can again be compensated for by increasing the number of channels for both figures of merit.

Of course, FN, SN, and random are not the only three

possible options for multiplexing-based policies. For example, one could develop a ranking scheme based on a combination of age and distance, or one could perform a search over all possible pairings of links, looking for the optimal pairings in terms of some figure of merit (such as the sum of lengths of all virtual links formed). With the respect to such optimal ranking schemes, it is not clear how close the SN and FN schemes are to being optimal; they are, however, simple and intuitive policy choices that require no optimization in terms of pairing of links for entanglement swapping, and hence are practical for near-term implementation. We defer the discussion of other policy alternatives and comments on the optimality of SN and FN SWAP-ASAP to Appendix D.

### A. Comparison to doubling

Let us now compare our policies with those in existing literature. In particular, we compare our policies with one widely studied in previous works, namely, the *doubling* (or *nesting*) policy; see, e.g., Refs. [15, 16, 58, 59, 64, 79]. In this policy, which only applies to repeater chains with  $2^N$  elementary links, the lengths of links are always doubled. As an example, consider the following situation. Suppose two adjacent elementary links are formed, an entanglement swap is performed successfully, and a link of length two is obtained. Now, in contrast to the SWAP-ASAP policy, this length-two link cannot be extended by swapping it with links of arbitrary lengths—links of length two must be swapped with links of length two only—which means that we must wait for another link of length two to be created before an entanglement swap can be attempted. In the meantime, the first produced virtual link keeps aging. We can thus see that this doubling policy is more restricted compared to SWAP-ASAP. Accordingly, it was shown in Ref. [75] that for low elementary link success probabilities and moderate swapping success probabilities (such as 50%, as in the case of linear optics), the SWAP-ASAP policy outperforms the doubling policy, although infinite coherence times for memories was assumed in that work.

Now, within the multiplexing scenario, the doubling policy can be implemented by ranking links based on age when more than one option of entanglement swapping is available. Thus, we call this policy *Strongest-Neighbor doubling* or SN doubling. Our aim now is to see if, within the multiplexing setting, and with finite coherence times for the quantum memories, our FN and SN SWAP-ASAP policies can outperform a doubling based multiplexing policy. This is what we show in Fig. 7. In terms of the average waiting time, the FN SWAP-ASAP policy outperforms the SN doubling policy for all values of link success probability  $p_\ell$  up to  $p_\ell = 0.5$ , including very low values of  $p_\ell$ , which is often most relevant in practice. It is important to mention here that this result is not true for all parameter regimes; for high values of  $p_\ell$  and  $m^*$ , the doubling policy can actually outperform our SWAP-ASAP policies. Our results are consistent with the results in previous works. Specifically, our results generalize those in Ref. [75] to the case of finite coherence times.

At the same time, our results also show the importance of

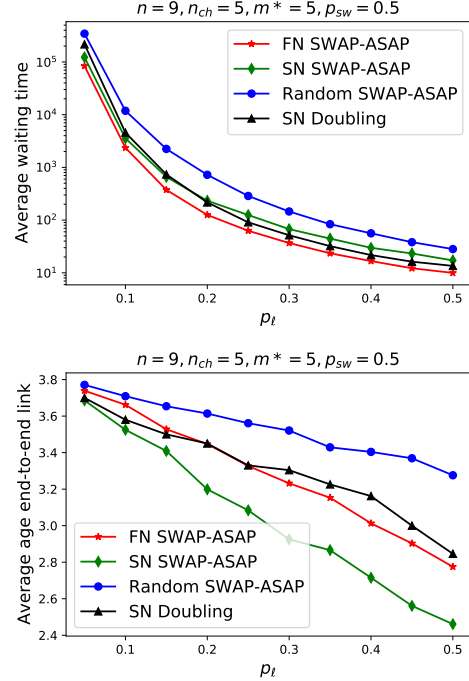


FIG. 7. Average waiting time (top) and average age of the youngest end-to-end link (bottom) for a repeater chain with  $n = 9$  nodes (eight elementary links), according to the FN, SN, and random SWAP-ASAP policies, compared to the SN doubling policy. For small values of  $p_\ell$ , both the FN and SN SWAP-ASAP policies outperform the doubling policy in terms of waiting time. The SN SWAP-ASAP policy outperforms doubling for the average age for all values of  $p_\ell$  up to  $p_\ell = 0.5$ .

ranking the links in an appropriate way, reflected in the fact that the *random* SWAP-ASAP policy and the SN SWAP-ASAP policies actually perform worse than the doubling policy in terms of average waiting time. We see very similar results in terms of the average age of the youngest end-to-end link. With respect to this figure of merit, the SN SWAP-ASAP policy outperforms all other policies discussed here, including the SN doubling policy. Below, in Sec. V, we also include distillation in our SWAP-ASAP policies and the doubling policy to compare their performance, since the latter has also been widely discussed in existing literature; see, e.g., Refs. [15, 16, 58, 59, 64, 79]. The doubling policy is also *quasi-local* in the same sense as SN and FN SWAP-ASAP, because a node needs to know the length of its links, i.e., it needs to know which nodes it is connected to. This is an important consideration when accounting for classical communication overheads of this policy, which we do in Sec. VI.

## V. MULTIPLEXING POLICIES WITH ENTANGLEMENT DISTILLATION

We now consider entanglement distillation with the probabilistic BBPSSW protocol [53], which allows for distillation of two entangled links to one. We provide a summary of the protocol in Appendix B. Briefly, if  $f_1$  and  $f_2$  are the

fidelities of the two links being distilled, then the success probability  $P_{\text{distill}}(f_1, f_2)$  of the protocol and the resulting fidelity  $F_{\text{distill}}(f_1, f_2)$  are given by

$$P_{\text{distill}}(f_1, f_2) = \frac{8}{9}f_1f_2 - \frac{2}{9}(f_1 + f_2) + \frac{5}{9}, \quad (2)$$

$$F_{\text{distill}}(f_1, f_2) = \frac{1 - (f_1 + f_2) + 10f_1f_2}{5 - 2(f_1 + f_2) + 8f_1f_2}. \quad (3)$$

The purpose of this section is to assess the usefulness of entanglement distillation for quantum repeater chains with multiple memories per repeater. In particular, in this section, we examine the extent to which entanglement distillation can compensate for the loss of fidelity incurred due to entanglement swapping and waiting (decoherence).

### A. Initial considerations

Recall that entanglement swapping of two links of ages  $m_1$  and  $m_2$  results in a virtual link of age  $m_1 + m_2$ , and waiting increases the ages of all active links by one time unit. Similarly, as we show in Appendix B, the age after distillation with the BBPSSW protocol is given by the following formula:

$$m' = \left\lceil m^* \log \left( \frac{15 - 6(f(m_1) + f(m_2)) + 24f(m_1)f(m_2)}{32f(m_1)f(m_2) - 2(f(m_1) + f(m_2)) - 1} \right) \right\rceil, \quad (4)$$

where  $m_1$  and  $m_2$  are the ages of the two links being distilled, the function  $f(m)$  is defined in Eq. (1), and  $\lceil x \rceil$  is the smallest integer greater than or equal to  $x$ .

We begin by noting that entanglement distillation is useful and worthwhile only when it increases the fidelity of the distilled link as compared to the fidelities of the original two links. In particular, the fidelity after distillation should be greater than the highest-fidelity link of the two being distilled, i.e.,  $F_{\text{distill}}(f_1, f_2) > \max\{f_1, f_2\}$ . In terms of ages, this translates to the following condition for entanglement distillation with the BBPSSW protocol to be useful:  $m' < \min\{m_1, m_2\}$ , where  $m'$  is the age after distillation, as given by Eq. (4). If  $m' \geq \min\{m_1, m_2\}$ , then we might as well use the youngest of the two links rather than attempt entanglement distillation and risk its failure. In particular, if one of the ages is 0, corresponding to a perfect Bell pair, then distillation should not be performed.

Another important consideration is that both links being distilled should be entangled. If one of the links is not entangled, then it is better to simply discard the unentangled link and keep the entangled one. We elaborate on this point in Appendix B. With this in mind, let us note that under the Pauli noise model that we consider, the fidelity according to Eq. (1) is bounded from below by 0.25 (in the limit  $m \rightarrow \infty$ ), and it is equal to approximately 0.5259 when  $m = m^*$ . The entanglement threshold for the states that we consider is 0.5, meaning that the link is entangled if and only if its fidelity strictly exceeds 0.5, and thus the age at which the link is no longer entangled is  $m = \lceil m^* \log(3) \rceil \approx \lceil 1.09m^* \rceil$ ; see Appendix A for the details. This means that, depending on the value of  $m^*$ , it can be useful to distill links that are older than  $m^*$  time steps. However, the probability of successful distillation falls with increasing ages

of the links, and hence using a very old link in conjunction with a very young link increases the likelihood of wasting the high-quality young link. Thus, while distillation might be useful in this scenario, it is not necessarily worthwhile. Also, for the moderate values of  $m^*$  considered in our simulations, we choose to discard links at  $m^*$  time steps, instead of the strict limit of  $\lceil m^* \log(3) \rceil$ , even when distillation is considered.

### B. Distillation policies

Now, when there are multiple (more than two) links that can be distilled, and we consider the pairwise BBPSSW protocol, the question of what is the optimal *distillation policy* naturally arises, i.e., what is the optimal pairing of links when performing entanglement distillation of more than two links. This question has been addressed in existing literature; see, e.g., Refs. [16, 79]. Here, we consider the following policies.

- *Banded policy*: Referred to as “scheme A” in Ref. [16], this involves distillation of entangled pairs that have the same age. Assuming that  $n_{ch}$  is a power of two, and assuming that all initial  $n_{ch}$  pairs have the same fidelity, they are all put into pairs and a first round of  $\frac{n_{ch}}{2}$  distillation attempts is made. The resulting links are all of the same fidelity and are paired again such that, in the next round,  $\frac{n_{ch}}{4}$  distillation attempts are made. This procedure continues for  $\log_2(n_{ch})$  rounds, at the end of which we have one link remaining. Assuming all of the initial links have fidelity  $f_0$ , the fidelity after  $r$  rounds is given by the recurrence relation  $f_r = F_{\text{distill}}(f_{r-1}, f_{r-1})$ . It has been shown in Ref. [16] that, as long as the initial links are all entangled ( $f_0 > \frac{1}{2}$ ), this policy can achieve arbitrarily high fidelities with an increasing value of  $n_{ch}$ .
- *Pumping policy*: Referred to as “scheme C” in Ref. [16], this policy proceeds as follows. Two links of fidelity  $f_0$  are distilled, then a fresh link of fidelity  $f_0$  is used to distill the previously distilled link, and so on. This policy is tailored to a practical situation in which fresh links are used to distill the surviving links of previous time steps, and thus the links being distilled do not necessarily have the same fidelity, as in the banded policy. If the initial fidelity satisfies  $f_0 > \frac{1}{2}$ , the fidelity  $f_r$  after  $r \in \{1, 2, \dots\}$  rounds of the pumping policy is given by the recurrence relation  $f_r = F_{\text{distill}}(f_{r-1}, f_0)$ . In Appendix B 1, we provide a closed-form, analytical solution to this recurrence relation, and using that solution we show that in the limit of arbitrarily many rounds of pumping, the fidelity saturates as follows:

$$\lim_{r \rightarrow \infty} f_r = \frac{6f_0 - 3 + \sqrt{7 - 26f_0 + 28f_0^2}}{8f_0 - 2}. \quad (5)$$

The limiting fidelity on the right-hand side of this equation is strictly less than one whenever  $f_0 < 1$ . This proves that, in contrast to the banded policy, with the pumping policy it is not possible to distill links to arbitrarily high fidelity, even with an infinite number of rounds.



- *Distill as soon as possible*: This is a sequential policy, which we introduce in this work as a hybrid of the banded and pumping policies, and very similar in spirit to the greedy policy defined in Ref. [79]. We sort the links in increasing order of their ages, and then pair them in increasing order. After one round of pairwise distillation, successfully distilled links are again sorted age-wise and the distillation is attempted again, until only one distilled link or no active link remains. This approach therefore uses the benefits of the banded policy, by pairing links of very similar ages, and at the same time, by realising the restrictions introduced by decoherence and finite number of channels, by pumping fresh links into the queue of available links as soon as possible. We therefore refer to this policy as “distill-as-soon-as-possible” (DISTILL-ASAP), and this is the policy that we consider for our simulations in Sec. VC below.

Now, how should we combine entanglement distillation with entanglement swapping? Should we distill first then swap—a policy we call DISTILL-SWAP—or the other way around, which we refer to as SWAP-DISTILL? In Appendix B 2 and Appendix C, we provide analytical calculations that compare the two policies for a three-node chain. For the rest of this section, we compare the policies with full-fledged simulations of long quantum repeater chains.

### C. Distill-swap vs. swap-distill: simulation results

Having developed some intuition about the performance of the distillation based policies through analytical results, let us now consider the fully dynamic setting with long quantum repeater chains. Here, the policy that we use is the DISTILL-ASAP policy defined in Sec. VB above. We stress again that the aim here is not to show optimality of our approach. The pairing of links for distillation is an optimization problem in its own right and not the focus of this work.

We now present simulation results for a five-node chain with five channels. A somewhat large value of the cutoff is chosen ( $m^* = 24$ ) to show some important scaling behaviour with increasing age  $m_0$  of the fresh (newly created) links. Fig. 8 shows the average waiting time and average age of end-to-end links as a function of the ages of the elementary links  $m_0$  when they are fresh, i.e., newly created. For both SWAP-DISTILL and DISTILL-SWAP, we have fixed the entanglement swapping policy to FN SWAP-ASAP.

It is clear that SWAP-DISTILL is the policy of choice in terms of reducing the waiting time when fresh elementary links have high fidelity (low age); otherwise, DISTILL-SWAP performs better. At the same time, DISTILL-SWAP always performs better in terms of the age of the end-to-end link. This result reinforces our intuition, developed from the previous analytical results. We also verify that waiting time rapidly increases beyond a threshold value of  $m_0$  for both SWAP-DISTILL and DISTILL-SWAP, the threshold being smaller for SWAP-DISTILL. Beyond the  $m_0$  values reported in Fig. 8, end-to-end entanglement generation time increases so much in the simulations that we are unable to find any reasonable estimate of an average value. Thus, for all

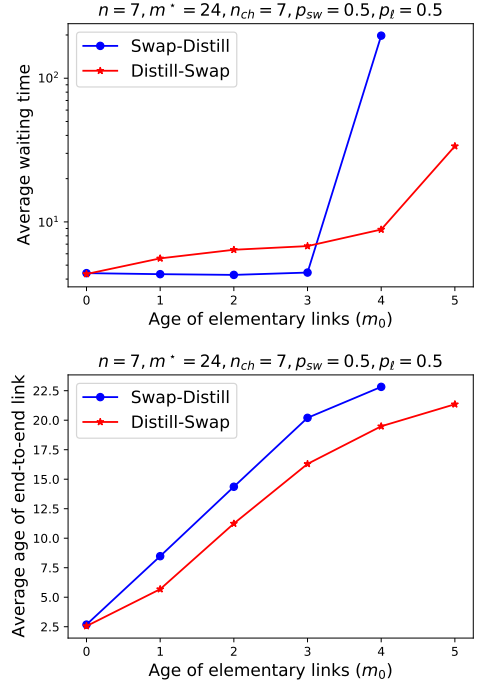


FIG. 8. Average waiting time (top) and average age of end-to-end links (bottom) as a function of the age  $m_0$  of newly-created elementary links. The entanglement swapping policy is fixed to FN SWAP-ASAP. It is clear that SWAP-DISTILL is the policy of choice in terms of reducing the waiting time when fresh elementary links have high fidelity (low age); otherwise, DISTILL-SWAP performs better.

practical purposes, the waiting time is essentially infinite. This is also indicated by the average ages approaching  $m^*$ .

Some estimates of the thresholds up to which the two distillation policies are effective can be made using some rather simple arguments. If the fresh elementary links have age  $m_0$ , the age of the distilled link saturates to a minimum value  $m_{min}^d(m_0)$  which is a function of  $m_0$ . In order to get an end-to-end link via entanglement swapping of such distilled links, the following condition must be satisfied:

$$(n-1) \cdot m_{min}^d(m_0) \leq m^*. \quad (6)$$

For the configuration in Fig. 8, the above condition translates to  $m_{min}^d \lesssim 4$ , which in terms of  $m_0$  is  $m_0 \leq 5$ , and this is the value around which we see that the average waiting time diverges.

In the case of SWAP-DISTILL, a typical trajectory to get an end-to-end link would be to first perform  $(n-2)$  swaps to get links of age  $(n-1) \cdot m_0$ , which are then distilled to links of age  $m_{min}^d((n-1) \cdot m_0)$ . The threshold condition thus takes the following form:

$$m_{min}^d((n-1) \cdot m_0) \leq m^*, \quad (7)$$

but since distillation is ineffective when both links involved are above the cutoff age, this condition is equivalent to

$$(n-1) \cdot m_0 \leq m^*. \quad (8)$$

This also explains why the threshold is lower for SWAP-DISTILL, since  $m_{min}^d(m_0) \leq m_0$ . Again, for the configuration in Fig. 8,

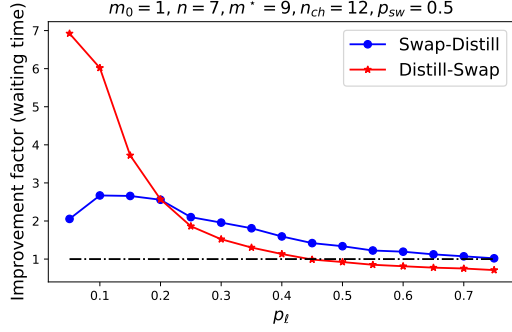


FIG. 9. Average waiting time improvement factor for distillation with the SWAP-DISTILL and DISTILL-SWAP policies (with FN SWAP-ASAP entanglement swapping). When  $p_\ell$  is low, DISTILL-SWAP performs better, and when  $p_\ell$  is high SWAP-DISTILL performs better. These are general trends and in concurrence with the Fig. 10 (center), where for low  $p_\ell$  DISTILL-SWAP is better but as  $p_\ell$  increases SWAP-DISTILL catches up. Furthermore, for large  $p_\ell$ , distillation is either not very useful, and can even be detrimental.

this translates to  $m_0 \lesssim 4$ , which agrees well with the simulation results. Furthermore, the threshold in the case of the SWAP-DISTILL policy is identical to a policy without distillation.

We further elaborate on our answer to the question of whether to distill first or to swap first in Fig. 9. We plot the waiting time improvement factor for distillation, which we define as the ratio of the average waiting time without distillation to the average waiting time with distillation. Apart from the quality of fresh links, as shown in Fig. 8, the choice between the two distillation policies also depends on the other network parameters. As an illustration, we show that for the parameters ( $n, n_{ch}, m^*, p_\ell$ ) chosen in Fig. 9, when  $p_\ell$  is low, DISTILL-SWAP performs better, and when  $p_\ell$  is high SWAP-DISTILL performs better. This can be understood in light of analytical results in Appendix C and Fig. 8. In the regime of low  $p_\ell$ , links are on average older and we have seen in the previous discussions in this section that DISTILL-SWAP performs better in this case since long entanglement swaps can only be possible once the ages of the participating links have been reasonably reduced; also, distilling after entanglement swapping is highly improbable to be successful because the ages are going to only increase due to the swapping. On the other hand, when  $p_\ell$  is high, SWAP-DISTILL performs better, because links are on average younger and much more conducive to successful entanglement swapping. Further we see that for large  $p_\ell$  distillation is either not very useful or even detrimental. Therefore, the decision to *distill* or not to *distill* also should be taken after considering the network parameters. We explore this point further in Fig. 10.

The discussion above leads us to the next question pertaining to the usefulness of distillation-based policies. We are yet to show whether there is any advantage in performing distillation. Distillation is a probabilistic process, and even when it succeeds it leads to a reduction in the number of active links. Hence, it is not manifest that a policy without distillation, such as SN or FN SWAP-ASAP alone, cannot perform better than its distillation-based counterpart. Let us look at two cases: when fresh elementary links are perfect, i.e.,  $m_0 = 0$ , and when they are

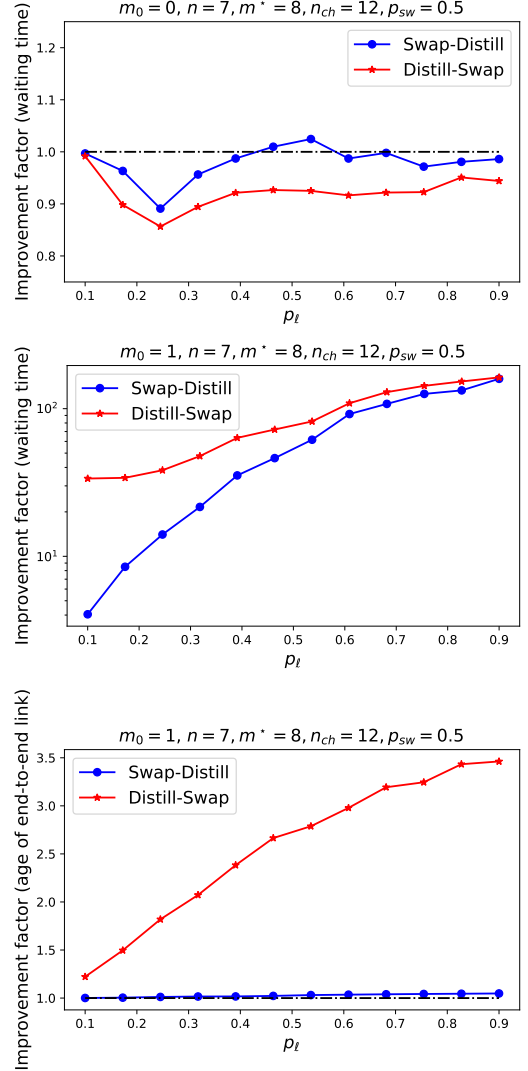


FIG. 10. Average waiting time improvement factor for distillation with the SWAP-DISTILL and DISTILL-SWAP policies (with FN SWAP-ASAP entanglement swapping). Distillation is not very useful, in fact mostly detrimental, when (top) fresh elementary links are perfect ( $m_0 = 0$ , 100% fidelity), but when fresh elementary links are imperfect (center) ( $m_0 = 1$ , approx. 90% fidelity), a dramatic reduction in waiting time can be obtained by performing distillation. (Bottom) Improvement factor for average age of youngest end-to-end link using distillation over non-distillation based (FN) policy. SWAP-DISTILL provides negligible advantage but DISTILL-SWAP provides substantial advantage.

imperfect, say  $m_0 = 1$  for concreteness. In Fig. 10 we look at a seven-node chain with  $n_{ch} = 12$  channels,  $p_{sw} = 0.5$ , and  $m^* = 8$  ( $m_0 = 1$  corresponds to roughly 90% fidelity in this case). We choose FN SWAP-ASAP as our swapping policy. We show the average waiting time improvement factor for distillation-based policies, defined as the ratio of average waiting time without distillation and with distillation as a function of the elementary link success probability  $p_\ell$ . An improvement factor of greater than 1 indicates an advantage in using distillation and vice versa. We see in Fig. 10 (top)

that distillation is mostly detrimental when freshly produced elementary links are perfect (100% fidelity). Both SWAP-DISTILL and DISTILL-SWAP increase the average waiting time, for all values of the elementary link probability. Further, the disadvantage is higher in the case of DISTILL-SWAP. This can be understood by the following observation. The primary role of distillation in the case when elementary links are perfect is to reduce the age of long or older links obtained as a consequence of waiting for other links and/or via entanglement swaps. The longest links tend to be the oldest ones in the network, due to the  $m_1 + m_2$  age-update rule for entanglement swapping. If we distill first, then initially, since most links are perfect, distillation is never invoked and after entanglement swaps, when distillation is needed, we have to wait an extra time step before distillation is attempted. This extra time step reduces the success probability of distillation of already old links, following Eq. (2). This is also the reason why SWAP-DISTILL has some positive improvement in some parameter regimes. Although not shown in Fig. 10, there exists a small parameter regime of low  $m^*$ ,  $p_\ell$  and  $n_{ch}$  in which SWAP-DISTILL leads to a small positive improvement (3-5%). The choice of parameters in the figure is motivated by the intent to show the most prominent and overarching trends. On the other hand, When elementary links are imperfect, distillation is essential in increasing the scale, fidelity and throughput of the network, indicated by the significant reduction in waiting time seen in Fig. 10 (bottom). When the elementary link probability is low, DISTILL-SWAP performs much better, and when it is high, SWAP-DISTILL catches up in terms of improvement. This is in agreement with the results shown in Fig. 8 and 9. Although, the trends of improvement factor variation with increasing elementary link probability change between Fig. 9 and 10. In terms of the end-to-end link fidelity SWAP-DISTILL provides negligible advantage but DISTILL-SWAP provides substantial advantage as shown in Fig. 10 (bottom).

#### 1. Comparison with the SN doubling policy

Let us now provide a comparison with the widely studied nested purification and doubling swapping policy. For this comparison, we fix the distillation order according to DISTILL-SWAP.

In Fig. 11 (top) we first consider the average waiting time. We see that, FN SWAP-ASAP outperforms doubling, similar to the results in Sec. III in terms of average waiting time. Furthermore, when considering at average age of the youngest end-to-end link, we see in Fig. 11 (bottom) that the SN SWAP-ASAP policy is able to outperform the SN doubling policy by providing higher end-to-end fidelity. These trends are similar to those obtained in Fig. 7 in Sec. III, and further establish the superiority of SWAP-ASAP based multiplexing policies over the doubling approach in generally resource-constrained settings, and more specifically when finite coherence times for quantum memories are considered.

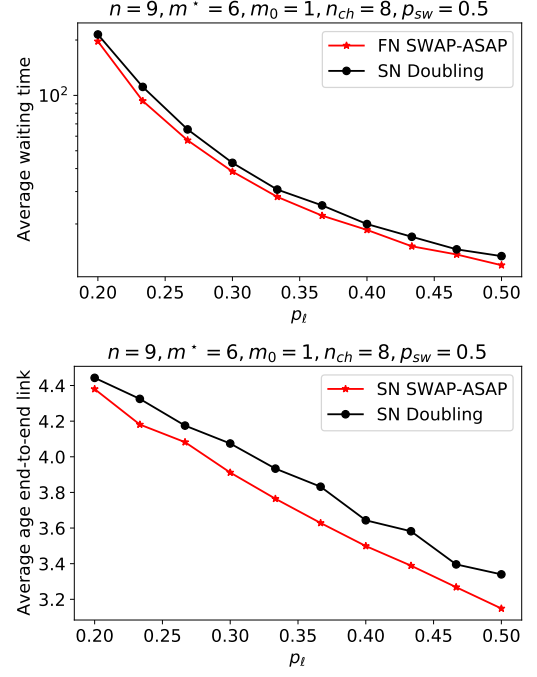


FIG. 11. Comparison between the SN doubling and FN and SN SWAP-ASAP policies with distillation according to DISTILL-SWAP. (Top) FN SWAP-ASAP provides smaller average waiting times than SN DOUBLING, similar to the results in Sec. III. (Bottom) The SN SWAP-ASAP policy is able to outperform the SN doubling policy when considering the average age of the youngest end-to-end link.

#### D. Main messages for distillation

In this section, we have addressed the following questions.

- *To distill or not to distill?*

*Yes*, when fresh elementary links are not perfect. In this case, distillation leads to a significant improvement in both the average waiting time and the average age of the end-to-end link.

*No*, when fresh elementary links are perfect. In this case, distillation offers either negligible advantage or is in fact detrimental for most parameter regimes.

More generally, the more resource constrained the scenario, i.e., in terms of network's hardware parameters, the more useful distillation is.

- *To distill first or to swap first?*

If links are generally low fidelity either due to low  $p_\ell$  or low initial fidelity, distilling first is more advantageous, in the opposite case it is better to swap first.

More generally, in resource constrained scenarios, i.e., in terms of network's hardware parameters, it is more useful to distill first and then swap.

## VI. CLASSICAL COMMUNICATION COST FOR MULTIPLEXING BASED SWAP-ASAP POLICIES

In a realistic near-term entanglement distribution setting with imperfect memories, considering classical communication (CC) costs is imperative. Since entanglement distribution at the elementary link level is not deterministic, it must be heralded via classical signals. This heralding sets a natural time scale for entanglement distribution through a network. The heralding time is equal to the classical communication time between two adjacent nodes. For the purposes of our simulation, this heralding time becomes the duration of one time step. Since entanglement swapping is also often probabilistic, two distinct classes of entanglement distribution approaches can be envisaged:

- A *local* approach, where all elementary link generation and entanglement swapping attempts are made agnostic of the success or failure of prior swaps. This would then mean that all elementary links (once generated successfully) are retained up to the cutoff time. When an entanglement swap has failed, resulting in both participating links to become inactive, the surrounding nodes must act as if the link is still active until it has reached its expected cutoff. All the classical communication about successful swaps is then done at the end of the protocol. Such an approach is fully local and therefore all policy decisions are taken by individual nodes, without any collaboration or exchange of information. The benefit is that no classical communication overheads exist except for heralding of elementary links, and therefore every time step has duration equal to the heralding time only. The cost is instead paid by having to wait for a link to reach its cutoff time, even though it might have become inactive long before that.
- A *global* approach, on the other hand, allows end-to-end classical communication amongst all nodes in every time step, such that the duration of every time step is equal to  $(n - 1) \times \Delta t$ , where  $\Delta t$  is the CC time across an elementary link. The waiting time is subsequently largely dominated by the CC overheads, putting a huge burden on the coherence time requirements of the memories. The benefit, of course, is that all nodes can now communicate with each other and take decisions collaboratively and in an adaptive fashion.

In previous works such as Refs. [42, 43], global policies were shown to optimize the average waiting time and fidelity; however, classical communication costs were not included. Furthermore, in Ref. [43], a “quasi-local” approach to entanglement distribution policies was proposed, in which there is knowledge of the network state up to some length scales only, and not globally. In this case, an advantage over fully local policies could still be obtained. We now investigate whether the advantages in waiting time and fidelity gained by global and quasi-local knowledge and collaboration can be retained when CC overheads are taken into account. The multiplexing based FN and SN SWAP-ASAP policies that we have introduced

in this work are quasi-local, and they have classical communication (CC) overheads. Indeed, whenever an entanglement swapping decision is made, all the memories at the node are assumed to have knowledge of which nodes/memories they are connected to. This information is needed to decide the order of entanglement swaps based on age (SN) or length (FN) of the links. Thus, every node has some “quasi-local” knowledge of the network state but not the “global” network state. In the previous sections, the CC overheads of the FN and SN SWAP-ASAP were not taken into account when determining the waiting time. Let us now take the CC overheads into account. We limit ourselves in this section to considering the FN and SN SWAP-ASAP policies without distillation, and hence the CC costs discussed will only be the ones associated with entanglement swapping.

Below is a summary of how we have taken classical communication into account in our model.

- In order to include the CC overheads, we approximate the CC time by adding  $t_{cc}$  time steps to every network evolution time step, where  $t_{cc}$  is determined by the length of the longest link involved in any entanglement swap occurring in that step. This allows enough time for the classical communication for all entanglement swaps attempted in that time step, and at the end of such a CC-accounted time step, all nodes are aware of which nodes they are connected to and the ages of those links (which can also be classically communicated). This is an upper bound to the CC cost, since in practice nodes could perform the next required action as soon as they receive the CC tagged for or relevant to them.
- In order to benchmark our quasi-local policies fairly against fully-local policies, some modifications need to be made to the way the network evolves under the fully-local policies. These modifications are necessary, because when entanglement swaps are probabilistic, if links need to be restarted after a failed Bell state measurement, but before their actual memory cutoff, some CC will be needed. Therefore, if a policy has to be fully-local and free of any CC overheads, nodes must be agnostic to entanglement swapping failures. All nodes, once they have a heralded entangled link, must retain them until their anticipated memory cutoff age  $m^*$ . Once this restriction is made, the only available information to nodes that can be used to decide the rank of states is the perceived or local ages of its memories. In other words, every link in the network now has two ages: one is its real age, as determined by probabilistic swaps in the evolution “in real-time”; the second is its *perceived* age, which is the age that the nodes that hold the link assume without any knowledge of the outcomes of entanglement swaps. When the perceived ages are used to take policy decision in the network, there is no CC overhead during the evolution. We call such a policy *local age-based* (ranking) multiplexed SWAP-ASAP policy. For such a policy, the CC cost is given by only one round of end-to-end communication time, in the last time step.

Having discussed our models for classical communication,



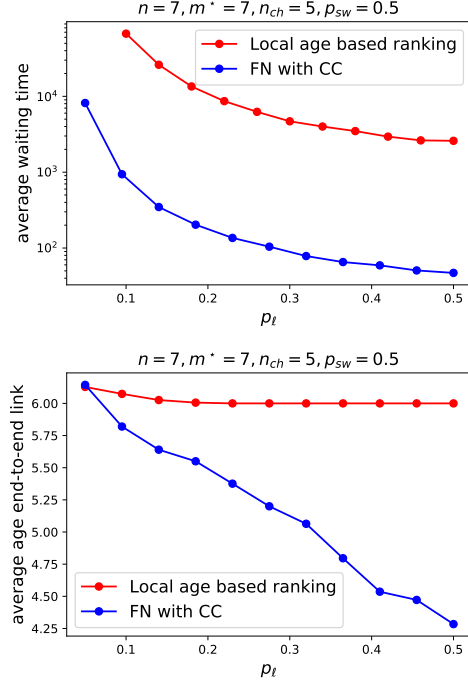


FIG. 12. Average waiting time (top) and average age of an end-to-end link (bottom) as a function of the elementary link success probability when classical communication times are included. We compare the quasi-local FN SWAP-ASAP policy with the fully-local age-based SWAP-ASAP policy. The FN SWAP-ASAP policy provides smaller values for both figures of merit even when CC costs are included. Similar trends can also be seen for the SN SWAP-ASAP policy.

before presenting simulation results, let us make a brief remark. In a full simulation, such as those which can be done via quantum network simulators such as NetSquid [35], QuISP [38], SeQuENCe [36], etc., time stamps are assigned to each quantum operation and tasks are queued, such that classical communication costs are intrinsically kept track of. Our simulations focus on optimization of policies, similar in spirit to *rule sets* used by many of the above mentioned simulators; see also Refs. [80, 81]. The task that we undertake here is highlighting that CC costs are relevant to the performance of policies or rule sets for entanglement distribution in a realistic setting.

Let us first look at the average waiting time and average age of the end-to-end link for the FN SWAP-ASAP policy when CC costs are included, as a function of the elementary link success probability. As mentioned above, we benchmark this policy against the local age-based SWAP-ASAP policy. From Fig. 12, it is clear that substantial advantage in terms of both figures of merit is retained even when CC times are taken into consideration.

A more surprising observation is the fact that even as the number of nodes increases, the advantage of FN SWAP-ASAP over the local age-based ranking policy remains strong—in fact, the advantage increases with an increasing number of nodes. In Fig. 13 (top), we show the average waiting times for the local age-based ranking and the FN SWAP-ASAP policies as a function of the number of nodes. Intuitively, we might

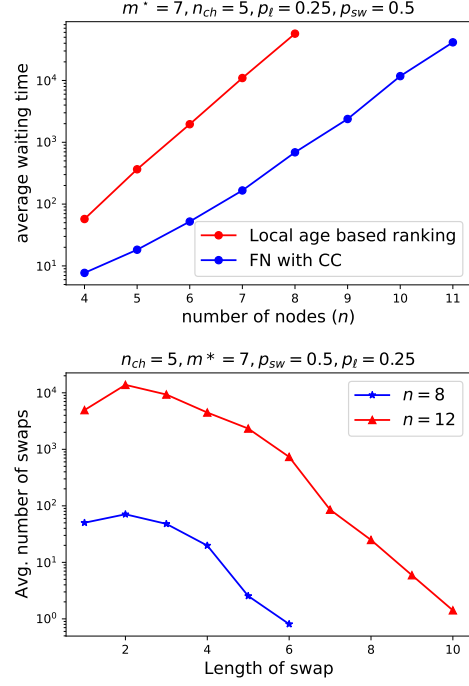


FIG. 13. (Top) Average waiting time as a function of the number of nodes when classical communication times are included. We compare the quasi-local FN SWAP-ASAP policy with the fully-local age-based SWAP-ASAP policy. The FN SWAP-ASAP policy provides smaller waiting times, even when CC costs are included. More surprisingly the advantage grows with an increasing number of nodes. This provides evidence of the scalability of the advantage gained by using knowledge of the network state. (Bottom) Number distribution of lengths of entanglement swaps in the FN SWAP-ASAP policy. We observe an exponential suppression of entanglement swaps of the order of the length of the chain, which is an important reason for the retained advantage of this policy, even with classical communication included.

have guessed that as the number of nodes increases, so too would the CC cost, because longer and longer swaps would be required to distribute entanglement between the end points of the chain, making quasi-local policies worse off in terms of average waiting times. It is therefore surprising that not only a large improvement using the FN and SN SWAP-ASAP policies is obtained for long chains, but further that the improvement increases with the growing scale (number of nodes) of the network.

Nonetheless, we can explain this non-intuitive result as follows. First, we remind the reader that although fully-local policies have the advantage of no CC overheads, they suffer in terms of average waiting time because due to the agnostic entanglement swapping. Waiting to restart links that are already dead is detrimental to the average waiting time. Second, a quasi-local policy, as the name suggests, is not fully global, and hence CC costs in a given time-step are upper-bounded by the length of the longest entanglement swapping operation. We define the length of an entanglement swapping operation as the length (in terms of number of nodes) of the longer of two links involved in the swap. In a typical trajectory of a network,

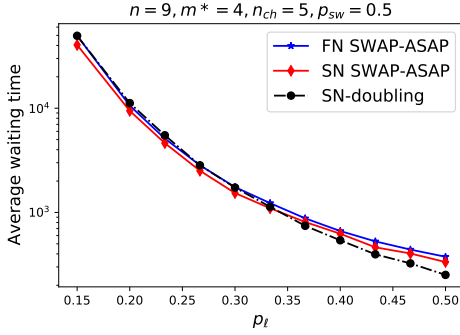


FIG. 14. Comparison of average waiting times for different quasi-local policies when classical communication costs are included. In the parameter regime selected for this example, reflecting a relatively resource-constrained scenario, SN SWAP-ASAP outperforms both FN SWAP-ASAP and SN doubling for the low elementary link success probability ( $p_\ell$ ) regime. This could be attributed to preference given to shorter swaps by SN and hence the avoidance of large CC costs. On the other hand, when  $p_\ell$  is larger, SN doubling performs the best, followed by SN SWAP-ASAP and then by FN SWAP-ASAP. Therefore, in this regime it is better to perform moderately longer swaps to minimize the waiting time.

from completely disconnected to an end-to-end connected link, for the FN SWAP-ASAP policy, the number of entanglement swapping operations of length equal to the number of nodes is roughly  $O(1)$ , i.e., roughly constant with respect to the number of nodes. This is seen in Fig. 13 (bottom). The average number distribution of the length of entanglement swaps shows an exponentially suppressed tail (linear fall on the logarithmic scale). Therefore, time steps in a typical MDP trajectory that contribute the highest to the CC overhead are rare. This justifies and supports the use of quasi-local policies over global policies for large networks, because in the latter, the CC cost is equal for each time-step and equal to the full network size, while for quasi-local policies the CC cost can be considerably less.

#### A. Comparison amongst quasi-local policies

We now compare the performance of different quasi-local policies when classical communication (CC) costs are included. We saw in Fig. 7 that the FN SWAP-ASAP policy provided the smallest waiting time amongst all quasi-local policies and thus also outperformed the doubling policy. Further, we observed that SN SWAP-ASAP performed worse than both SN doubling and FN SWAP-ASAP in terms of the average waiting time for end-to-end connection. With CC costs included, new interesting trends emerge in a very similar resource-constrained scenario, as shown in Fig. 14. First, in the low  $p_\ell$  regime, we see that it is SN SWAP-ASAP that provides the smallest waiting time, followed by FN SWAP-ASAP, and then very closely followed by SN doubling. This result can be attributed to the preference given to the shortest swaps (youngest links are generally the shortest ones) by SN SWAP-ASAP compared to both the FN SWAP-ASAP and SN doubling policies. Consequently, SN SWAP-ASAP is able to avoid any large CC costs. In a scenario of

low  $m^*$ , as considered in this example, when  $p_\ell$  is also low, most links are already very close to their cutoff time when an entanglement swap can be attempted; thus, it is essential to avoid any large CC costs, thus making SN SWAP-ASAP the policy of choice. On the other hand, when  $p_\ell$  is larger, SN doubling performs the best, followed by SN SWAP-ASAP, and then by FN SWAP-ASAP. This result can be attributed to the fact that, in this regime, it is better to perform moderately longer swaps to minimize the waiting time. As mentioned above, we have not considered distillation-based policies here, since our model does not account for CC costs associated with distillation.

## VII. PROPOSED EXPERIMENTAL IMPLEMENTATION

Based on the multiplexed model introduced in Fig. 1, in this section we propose a proof-of-principle experimental realization of a quantum network with multiplexing using a high-dimensional biphoton frequency comb (BFC) in Fig. 15. First, the BFC state is prepared by passing the spontaneous parametric down-conversion (SPDC) photons generated from a type-II periodically-poled KTiOPO4 (ppKTP) waveguide through a fiber Fabry-Pérot cavity (FFPC) [82, 83]. Due to the type-II phase-matching condition, the signal and idler photons can be efficiently separated by a polarization beam-splitter (PBS), enabling deterministic BFC generation without post-selection. The signal and idler photons are then temporally overlapped at a fiber beamsplitter with orthogonal polarizations, by using a tunable delay line (DL) and polarization controllers [82]. This configuration generates polarization entangled BFC state

$$|\psi\rangle = \sum_{m=-N}^N |\omega_p/2 + m\Delta\Omega\rangle_1 |\omega_p/2 - m\Delta\Omega\rangle_2 \otimes (|H\rangle_1 |V\rangle_2 + |V\rangle_1 |H\rangle_2), \quad (9)$$

where  $2N + 1$  is the number of cavity lines passed by an overall bandwidth-limiting filter (the number of frequency modes),  $\Delta\Omega$  is the free spectral range of the FFPC, and  $\omega_p$  is the pump frequency [83]. This scalable frequency-polarization hyperentangled BFC state [82] facilitates the multiplexing network policy by transmitting polarization qubits via different frequency channels to quantum network nodes, where entanglement swapping is performed in polarization basis. Specifically, within the context of our theoretical model,  $n_{ch} = 2N + 1$ . As shown in Fig. 15(a), one output channel of the beamsplitter is directed to Bob, and the other is connected to a commercial dense wavelength-division multiplexing (DWDM) module for de-multiplexing and sent to quantum network nodes, consisting of multiple quantum memories. Each frequency channel is assigned to couple to one quantum memory at the quantum network node. The entanglement swapping inside a node is assisted by an auxiliary SPDC source, where the signal photons are sent to Bell-state measurement and idler photons are sent to another memory to establish a fiber link to the next node.

Fig. 15(b) shows the measured frequency correlation matrix of a BFC, using a FFPC of 50 GHz free spectral range (FSR) and finesse of 10. We measured 9 correlated frequency-bin pairs

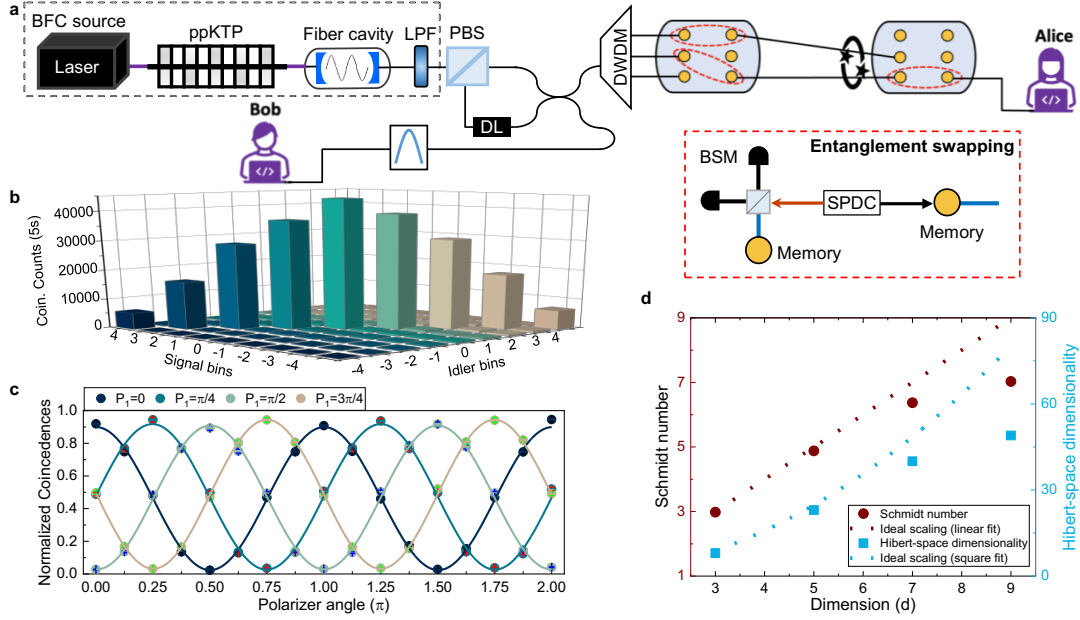


FIG. 15. (a) Proposed implementation of multiplexing policy using a high-dimensional biphoton frequency comb. (b) Measured frequency correlation matrix of the biphoton frequency comb. (c) Polarization entanglement measurements of a biphoton frequency comb. (d) Schmidt number and Hilbert-space dimensionality scaling for different dimensions in a biphoton frequency comb.

between signal and idler photons with a type-II SPDC source of  $\approx 250$  GHz phase-matching bandwidth. Fig. 15(c) shows the measured high-quality polarization fringes for the BFC state before de-multiplexing, which shows a raw fringe visibility up to  $94.1 \pm 0.5\%$  and violates the Clauser-Horne-Shimony-Holt (CHSH) inequality by 19 standard deviations with score  $S = 2.666 \pm 0.034$ . This polarization state yields a state fidelity of  $93.3 \pm 0.1\%$  with respect to a Bell state  $\frac{1}{\sqrt{2}}(|H\rangle_1|V\rangle_2 + |V\rangle_1|H\rangle_2)$ . Such high-fidelity polarization entanglement facilitates the entanglement swapping between quantum memories.

We perform the Schmidt mode decomposition of the measured joint spectral intensity [82], and summarize the extracted Schmidt mode number ( $K$ ), and the corresponding Hilbert space dimension ( $K^2$ ). When reconstructing the density matrix, we observe that the Schmidt mode number and Hilbert-space dimension scales with the dimension  $d$  of the biphoton frequency comb, as shown in Fig. 15(d). The Schmidt mode number is 2.98 with  $d = 3$ , and  $K = 7.03$  when we increase the dimension to  $d = 9$ . The deviation from ideal scaling in Fig. 15(d) mainly comes from the sinc function of the SPDC spectrum, which can be circumvented by using a flat-top broadband SPDC source. The Hilbert-space dimension can be further increased by using a SPDC source with broader spectrum bandwidth and FFPC with smaller FSR. We also note that by passing only the signal photons through a FFPC, the idler photons will still exhibit a comb-like behavior [84, 85]. Such a scheme can provide higher photon flux due to less filtering loss, and with potentially higher secure key rates for quantum key distribution [86–88]. Although we have already experimentally implemented the multiplexed source required for the proposed experimental implementation, integration of the scheme with quantum memories, implementing entanglement swapping, and distillation of

links has not been done yet. At the same time, there has been great progress in each of these key steps for the construction of a long-distance quantum network.

#### A. Calculation of elementary link probability, time step, and memory cutoff

In this section, we show how to translate physical parameters into the values of  $p_\ell$ ,  $m^*$ , and  $\Delta t$  within our theoretical framework

*Elementary link success probability  $p_\ell$ .* In general, we have that

$$p_\ell = \eta_r \eta_\ell \eta^2, \quad (10)$$

where  $\eta_\ell = \exp(-\frac{\ell}{12 \text{ km}})$  is the photon-loss contribution, with  $\ell$  being the length of the elementary link. For  $\ell = 40$  km, we have  $\eta_\ell \approx 0.036$ . The factor of  $\frac{1}{12 \text{ km}}$  in the exponent corresponds to the 3.63 dB loss in the 10 km channel reported in the experiment in Ref. [85]. In addition,  $\eta = 0.69$  is the Debye–Waller factor, the ideal efficiency of the memory (fraction of photons captured in the memory out of all the incident photons) [89], for a rare-Earth metal based quantum memory [90], and  $\eta_r = 0.79$  (approximately 1 dB) is the loss from other residual factors, which could include detector efficiencies, optical component loss, etc. [82]. Altogether, we have that  $p_\ell = \eta_r \eta_\ell \eta^2 \approx 0.0134$ .

*Heralding time step  $\Delta t$ .* This is given by the elementary link distance  $\ell$  as

$$\Delta t = \frac{n\ell}{c} \text{ seconds}, \quad (11)$$

$\ell$ (km)	$p_\ell$	$\Delta t$ (ms)	$m^\star$
25.0	0.05	0.125	8
15.0	0.11	0.075	13
5.0	0.25	0.025	40

TABLE I. Parameters  $p_\ell$ ,  $\Delta t$ , and  $m^\star$  of our theoretical model, calculated for varying elementary link distances  $\ell$  based on the physical aspects of the quantum channels and memories.

where  $n$  is the refractive index of the communication medium,  $\ell$  is length of the elementary link, and  $c$  is the speed of light in vacuum.

*Memory cutoff  $m^\star$ .* Using the memory coherence time of  $T_2 \approx 1$  ms, as for a rare-Earth metal based quantum memory [90], we can find the memory cutoff  $m^\star$  as

$$m^\star = \frac{T_2}{\Delta t}. \quad (12)$$

For  $\ell = 40$  km, we have  $m^\star = 5$ .

In Table I, we calculate our model parameters for various values of the elementary link distance.

### B. Figures of merit and repeater chain design for existing memory platforms

Let us now address the following question. Given a particular number  $n_{ch}$  of channels for multiplexing, and given other physical parameters corresponding to channel losses, quantum memory coherence times, etc., what is the optimal number of repeater nodes for a linear quantum repeater chain spanning a certain distance, and what would be the rate and fidelity of end-to-end entanglement distribution for this optimal setting? Intuitively, we do expect such an optimal number of nodes to exist, because as the number of nodes increases, even though the individual links become smaller and thus  $p_\ell$  and  $m^\star$  both increase, the non-deterministic nature of entanglement swapping will at some point begin to adversely affect the waiting time as the number of nodes increases.

To answer this question, let us set the end-to-end distance to be 100 km. We also use the FN SWAP-ASAP policy for illustrative purposes, and we also include the classical communication overheads, but we leave out distillation-based policies. We also let the entanglement swapping success probability be  $p_{sw} = 0.5$  and the number of channels for multiplexing be  $n_{ch} = 9$ . The other physical parameters are chosen to reflect the proposed experimental implementation above. For the quantum memories, we choose two state-of-the-art quantum memory platforms for our analysis, a rare-Earth metal based memory ( $\text{Pr}^{3+}$  ions) and a diamond vacancy based memory.

We plot the average waiting time and fidelity in Fig. 16. We tabulate the values for the fidelity and entanglement distribution rate for the two memory platforms in the optimal setting, along with the hardware parameters, in Table II. The optimal number of nodes in terms of the waiting time seems to be around five to seven for both memory platforms, which have  $T_2$  times on the order of a few milliseconds. From the minimum value of

Memory	$T_2$	$\eta$	$f_0$	$p_\ell$	$m^\star$	$m_0$	$R$	$f$
Rare-Earth	1.2 ms	0.69	0.98	0.046	9	0	200 Hz	0.72
Diamond	13 ms	0.20	0.89	0.008	156	24	50 Hz	0.74

TABLE II. Hardware parameters for two quantum memory platforms (rare-earth ion and diamond vacancy), and their respective optimal entanglement distribution rates ( $R$ ) and end-to-end fidelities ( $f$ ), for a 100 km repeater chain, based on the data in Fig. 16.  $T_2$  is the coherence time of the memory,  $\eta$  is the absorption efficiency (Debye–Waller factor), and  $f_0$  is the fidelity of a fresh elementary link. Also shown are the parameters  $p_\ell$ ,  $m^\star$ , and  $m_0$  of our theoretical model.

the waiting time, we anticipate entanglement distribution rates ranging from a few tens of Hertz to a few hundred Hertz, with an average end-to-end link fidelity of 70-75%. At the same time, for the end-to-end fidelity, the results of the two platforms do not have the same trends. For the diamond vacancy based memory, the fidelity seems to not have its minimum at around the same point as the waiting time, indicating a direct trade-off between the two figures of merit. On the other hand, for the rare-Earth metal based memory, the fidelity decreases with an increasing number of nodes.

## VIII. CONCLUSIONS AND DIRECTIONS FOR FUTURE WORK

In this paper, we have looked at practical multiplexing-based policies for long-distance entanglement distribution using quantum repeaters with multiple memories. We have proposed two paradigmatic policies, namely farthest neighbour (FN) SWAP-ASAP and strongest neighbour (SN) SWAP-ASAP, adapting swap-as-soon-as-possible policies for multiplexing-based linear networks. We have benchmarked these policies against a non-multiplexed, or parallel SWAP-ASAP policy, a policy that exploits multiplexing but does not use knowledge of the network state, and the widely studied doubling policy. We have shown via simulations that the FN and SN SWAP-ASAP policies can yield a considerable advantage over the alternative policies considered, both in terms of reducing the average waiting time increasing the fidelity of the end-to-end link. These advantages occur in the most relevant parameter regimes for near-term quantum networks, which correspond to the most resource-constrained settings.

We then considered policies with entanglement distillation, and we proposed a new policy that we call DISTILL-ASAP. This policy combines the benefits of existing distillation policies, like the banded, greedy and pumping approaches, and thus is able to outperform the well-studied DOUBLING policy nested with distillation. We also provide answers to two important policy questions related to distillation: When is distillation useful, and when it is useful, should we distill then swap, or the other way around? In this direction, the next question of immediate interest for future work is: “How much to distill?” Indeed, in this work, we only considered entanglement distillation policies that take  $N$  links and distill them to one, but one could instead distill  $N$  links to some  $K$  links greater than one, and such



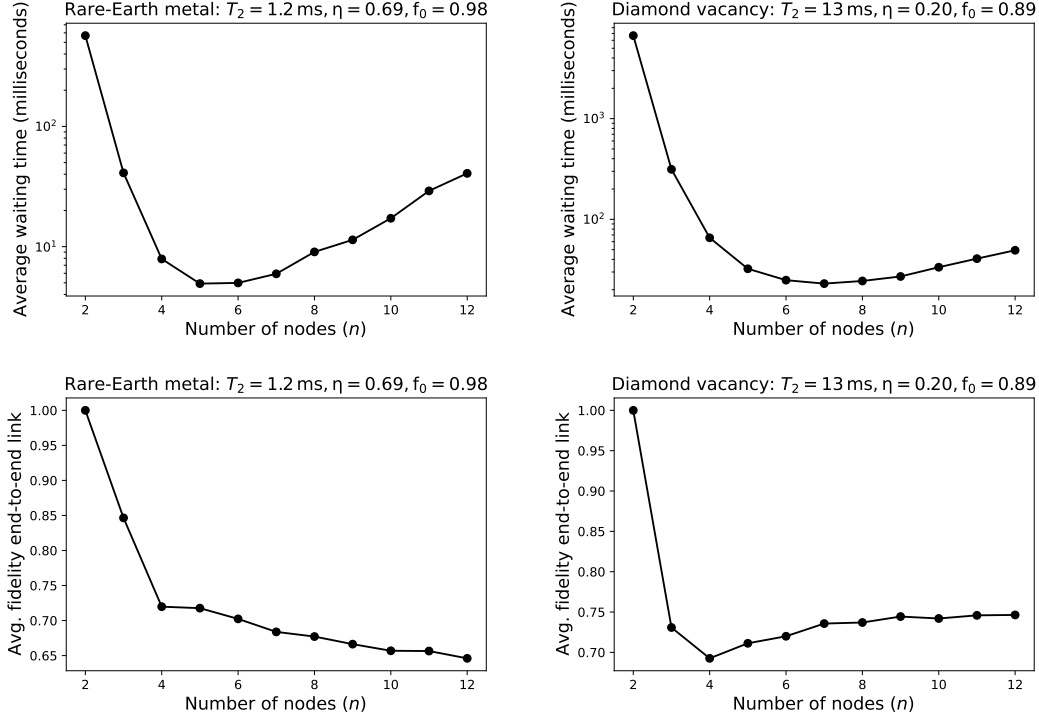


FIG. 16. Average waiting time (top), including classical communication overheads, and average fidelity of the end-to-end link (bottom) for entanglement distribution along a 100 km repeater chain with rare-Earth ( $\text{Pr}^{3+}$  ion) (left) and diamond vacancy (right) based memories using the FN SWAP-ASAP policy. Even though the  $T_2$  coherence times and elementary link probabilities are relatively low, multiplexed policies provide reasonable communication rates and end-to-end link fidelities. Using five to six repeaters between the end nodes seems to be optimal for both memories in terms of waiting times.

protocols have been the study of recent work [91].

An important consideration for practical and scalable implementation of entanglement distribution policies is the classical communication (CC) cost associated with non-deterministic entanglement swapping. Here, we have considered these overheads and shown that not only do multiplexed policies retain their advantage over non-multiplexed policies when CC costs are included, but this advantage can also increase with an increasing number of nodes. This is a surprising and counter-intuitive result, and shows that policies that use some knowledge of the network state (but not necessarily full, global knowledge) can enhance network performance even when CC costs associated with such knowledge are accounted for. This is a very important conclusion from the point of view determining useful policies beyond the fully-local ones, especially for large quantum networks. Our work provides much needed evidence in support of the widely believed conjecture that policies that utilize knowledge of the network state can outperform policies that do not use such information.

Finally, to make the numerical and analytical analyses of this work more concrete, we performed an experimental demonstration of multiplexing using a high-dimensional biphoton frequency comb (BFC), which would form the backbone of our proposed experimental implementation of a linear-chain quantum network with multiplexing capabilities. We then assessed

the anticipated performance of such a network over 100 km for two concrete memory platforms, namely rare-earth ion and diamond vacancy based quantum memories, when using our multiplexing-based policies.

A universal principle that is evident from the results of this work is that *policies must be tailored to the hardware parameters of the network*. This motivates us to further explore the question of policies, given that no single entanglement distribution policy can provide an advantage in all network scenarios.

## ACKNOWLEDGMENTS

The authors thank Thomas Searles and Sanjaya Lohani for helpful discussions. This work was supported by the Army Research Office Multidisciplinary University Research Initiative (ARO MURI) through the grant number W911NF2120214. SH also acknowledges support from the RCS program of Louisiana Boards of Regents through the grant LEQSF(2023-25)-RD-A-04, NSF grant PHY-2110273, funds from Xairos Inc., and funds from the Hearne Institute for Theoretical Physics. PB and HL also acknowledge the support of the U.S. Air Force Office of Scientific Research as well as the US-Israel Binational Science Foundation. SK acknowledges financial support from the German BMBF (Hybrid).

- 
- [1] S. Wehner, D. Elkouss, and R. Hanson, Quantum internet: A vision for the road ahead, *Science* **362** (2018).
- [2] J. Dowling, *Schrödinger's Web: Race to Build the Quantum Internet* (Taylor & Francis, 2020).
- [3] R. Van Meter, *Quantum Networking* (John Wiley & Sons, Ltd, 2014).
- [4] C. H. Bennett and G. Brassard, Quantum cryptography: Public key distribution and coin tossing, in *International Conference on Computer System and Signal Processing, IEEE* (1984) pp. 175–179.
- [5] F. Xu, X. Ma, Q. Zhang, H.-K. Lo, and J.-W. Pan, Secure quantum key distribution with realistic devices, *Reviews of Modern Physics* **92**, 025002 (2020).
- [6] J. I. Cirac, A. K. Ekert, S. F. Huelga, and C. Macchiavello, Distributed quantum computation over noisy channels, *Physical Review A* **59**, 4249 (1999).
- [7] S. Barz, E. Kashefi, A. Broadbent, J. F. Fitzsimons, A. Zeilinger, and P. Walther, Demonstration of blind quantum computing, *Science* **335**, 303 (2012).
- [8] W. Ge, K. Jacobs, Z. Eldredge, A. V. Gorshkov, and M. Foss-Feig, Distributed quantum metrology with linear networks and separable inputs, *Physical Review Letters* **121**, 043604 (2018).
- [9] P. Komar, E. M. Kessler, M. Bishof, L. Jiang, A. S. Sørensen, J. Ye, and M. D. Lukin, A quantum network of clocks, *Nature Physics* **10**, 582 (2014).
- [10] T. J. Proctor, P. A. Knott, and J. A. Dunningham, Multiparameter estimation in networked quantum sensors, *Physical Review Letters* **120**, 080501 (2018).
- [11] K. Heshami, D. G. England, P. C. Humphreys, P. J. Bustard, V. M. Acosta, J. Nunn, and B. J. Sussman, Quantum memories: emerging applications and recent advances, *Journal of Modern Optics* **63**, 2005 (2016).
- [12] D. Awschalom, K. K. Berggren, H. Bernien, S. Bhavé, L. D. Carr, P. Davids, S. E. Economou, D. Englund, A. Faraon, M. Fejer, S. Guha, M. V. Gustafsson, E. Hu, L. Jiang, J. Kim, B. Kozh, P. Kumar, P. G. Kwiat, M. Lončar, M. D. Lukin, D. A. Miller, C. Monroe, S. W. Nam, P. Narang, J. S. Orcutt, M. G. Raymer, A. H. Safavi-Naeini, M. Spiropulu, K. Srinivasan, S. Sun, J. Vučković, E. Waks, R. Walsworth, A. M. Weiner, and Z. Zhang, Development of Quantum Interconnects (QICs) for Next-Generation Information Technologies, *PRX Quantum* **2**, 017002 (2021).
- [13] M. Pompili, S. L. N. Hermans, S. Baier, H. K. C. Beukers, P. C. Humphreys, R. N. Schouten, R. F. L. Vermeulen, M. J. Tiggeleman, L. dos Santos Martins, B. Dirkse, S. Wehner, and R. Hanson, Realization of a multi-node quantum network of remote solid-state qubits, *Science* **372**, 259 (2021).
- [14] S. L. N. Hermans, M. Pompili, H. K. C. Beukers, S. Baier, J. Borregaard, and R. Hanson, Qubit teleportation between non-neighbouring nodes in a quantum network, *Nature* **605**, 663 (2022).
- [15] H.-J. Briegel, W. Dür, J. I. Cirac, and P. Zoller, Quantum Repeaters: The Role of Imperfect Local Operations in Quantum Communication, *Physical Review Letters* **81**, 5932 (1998).
- [16] W. Dür, H.-J. Briegel, J. I. Cirac, and P. Zoller, Quantum repeaters based on entanglement purification, *Physical Review A* **59**, 169 (1999).
- [17] O. A. Collins, S. D. Jenkins, A. Kuzmich, and T. A. B. Kennedy, Multiplexed Memory-Insensitive Quantum Repeaters, *Physical Review Letters* **98**, 060502 (2007).
- [18] N. K. Bernardes, L. Praxmeyer, and P. van Loock, Rate analysis for a hybrid quantum repeater, *Physical Review A* **83**, 012323 (2011).
- [19] K. Azuma, K. Tamaki, and H.-K. Lo, All-photonic quantum repeaters, *Nature Communications* **6** (2015).
- [20] F. Rozpędek, K. Goodenough, J. Ribeiro, N. Kalb, V. C. Vivoli, A. Reiserer, R. Hanson, S. Wehner, and D. Elkouss, Parameter regimes for a single sequential quantum repeater, *Quantum Science and Technology* **3**, 034002 (2018), 1705.00043.
- [21] S. Das, S. Khatri, and J. P. Dowling, Robust quantum network architectures and topologies for entanglement distribution, *Physical Review A* **97**, 012335 (2018).
- [22] S. Khatri, C. T. Matyas, A. U. Siddiqui, and J. P. Dowling, Practical figures of merit and thresholds for entanglement distribution in quantum networks, *Physical Review Research* **1**, 023032 (2019).
- [23] F. Rozpędek, R. Yehia, K. Goodenough, M. Ruf, P. C. Humphreys, R. Hanson, S. Wehner, and D. Elkouss, Near-term quantum-repeater experiments with nitrogen-vacancy centers: Overcoming the limitations of direct transmission, *Physical Review A* **99**, 052330 (2019).
- [24] S. E. Vinay and P. Kok, Statistical analysis of quantum-entangled-network generation, *Physical Review A* **99**, 042313 (2019).
- [25] E. Shchukin, F. Schmidt, and P. van Loock, Waiting time in quantum repeaters with probabilistic entanglement swapping, *Physical Review A* **100**, 032322 (2019).
- [26] B. Li, T. Coopmans, and D. Elkouss, Efficient Optimization of Cutoffs in Quantum Repeater Chains, *IEEE Transactions on Quantum Engineering* **2**, 1 (2021).
- [27] G. Vardoyan, S. Guha, P. Nain, and D. Towsley, On the exact analysis of an idealized quantum switch, *Performance Evaluation* **144**, 102141 (2020).
- [28] S. Khatri, *Towards a General Framework for Practical Quantum Network Protocols*, Ph.D. thesis, Louisiana State University (2021), [https://digitalcommons.lsu.edu/gradschool\\_dissertations/5456/](https://digitalcommons.lsu.edu/gradschool_dissertations/5456/).
- [29] T. Coopmans, *Tools for the design of quantum repeater networks*, Ph.D. thesis, Delft University of Technology (2021), <https://repository.tudelft.nl/islandora/object/uuid:90d06f1d-4f23-48cc-8f96-51500258020f?collection=research>.
- [30] L. Kamin, E. Shchukin, F. Schmidt, and P. van Loock, Exact rate analysis for quantum repeaters with imperfect memories and entanglement swapping as soon as possible, *arXiv:2203.10318* (2022).
- [31] T. Coopmans, S. Brand, and D. Elkouss, Improved analytical bounds on delivery times of long-distance entanglement, *Physical Review A* **105**, 012608 (2022).
- [32] W. Dai and D. Towsley, Entanglement Swapping for Repeater Chains with Finite Memory Sizes, *arXiv:2111.10994* (2021).
- [33] A. Sadhu, M. A. Somayajula, K. Horodecki, and S. Das, Practical limitations on robustness and scalability of quantum Internet, *arXiv:2308.12739* (2023).
- [34] X. You, X. Li, Y. Xu, H. Feng, and J. Zhao, Toward Packet Routing with Fully-distributed Multi-agent Deep Reinforcement Learning, in *2019 International Symposium on Modeling and Optimization in Mobile, Ad Hoc, and Wireless Networks (WiOPT)* (2019) pp. 1–8.
- [35] T. Coopmans, R. Knegjens, A. Dahlberg, D. Maier, L. Nijsten, J. Oliveira, M. Papendrecht, J. Rabbie, F. Rozpędek, M. Skrzypczyk, L. Wubben, W. de Jong, D. Podareanu, A. T. Knoop, D. Elkouss, and S. Wehner, NetSquid, a NETwork

- Simulator for QUantum Information using Discrete events, *Communications Physics* **4**, 164 (2021).
- [36] X. Wu, A. Kolar, J. Chung, D. Jin, T. Zhong, R. Kettimuthu, and M. Suchara, SeQUeNCe: a customizable discrete-event simulator of quantum networks, *Quantum Science and Technology* **6**, 045027 (2021).
- [37] J. Walln  fer, F. Hahn, F. Wiesner, N. Walk, and J. Eisert, Re-QuSim: Faithfully simulating near-term quantum repeaters, *arXiv:2212.03896* (2022).
- [38] R. Satoh, M. Hajdu  ek, N. Benchasattabuse, S. Nagayama, K. Teramoto, T. Matsuo, S. A. Metwalli, P. Pathumsoot, T. Satoh, S. Suzuki, and R. V. Meter, QuISP: a Quantum Internet Simulation Package, in *2022 IEEE International Conference on Quantum Computing and Engineering (QCE)* (2022) pp. 353–364.
- [39] F. F. da Silva, A. Torres-Knoop, T. Coopmans, D. Maier, and S. Wehner, Optimizing entanglement generation and distribution using genetic algorithms, *Quantum Science and Technology* **6**, 035007 (2021).
- [40] S. B  uml, K. Azuma, G. Kato, and D. Elkouss, Linear programs for entanglement and key distribution in the quantum internet, *Communications Physics* **3**, 55 (2020).
- [41] S. D. Rei   and P. van Loock, Deep reinforcement learning for key distribution based on quantum repeaters, *arXiv:2207.09930* (2022).
- [42]   lvaro G. I  esta, G. Vardoyan, L. Scavuzzo, and S. Wehner, Optimal entanglement distribution policies in homogeneous repeater chains with cutoffs, *npj Quantum Information* **9**, 46 (2023), 2207.06533.
- [43] S. Haldar, P. J. Barge, S. Khatri, and H. Lee, Fast and reliable entanglement distribution with quantum repeaters: principles for improving protocols using reinforcement learning, *arXiv:2303.00777* (2023).
- [44] N. Sangouard, C. Simon, H. de Riedmatten, and N. Gisin, Quantum repeaters based on atomic ensembles and linear optics, *Reviews of Modern Physics* **83**, 33 (2011), 0906.2699.
- [45] A. S. Cacciapuot  , M. Caleffi, F. Tafuri, F. S. Cataliotti, S. Gherardini, and G. Bianchi, Quantum Internet: Networking Challenges in Distributed Quantum Computing, *IEEE Network* **34**, 137 (2020), 1810.08421.
- [46] A. S. Cacciapuot  , M. Caleffi, R. Van Meter, and L. Hanzo, When Entanglement Meets Classical Communications: Quantum Teleportation for the Quantum Internet, *IEEE Transactions on Communications* **68**, 3808 (2020), 1907.06197.
- [47] K. Azuma, S. B  uml, T. Coopmans, D. Elkouss, and B. Li, Tools for quantum network design, *AVS Quantum Science* **3**, 014101 (2021).
- [48] W. J. Munro, N. L. Piparo, J. Dias, M. Hanks, and K. Nemoto, Designing tomorrow’s quantum internet, *AVS Quantum Science* **4**, 020503 (2022).
- [49] J. Illiano, M. Caleffi, A. Manzalini, and A. S. Cacciapuot  , Quantum Internet protocol stack: A comprehensive survey, *Computer Networks* **213**, 109092 (2022).
- [50] K. Azuma, S. E. Economou, D. Elkouss, P. Hilaire, L. Jiang, H.-K. Lo, and I. Tzitrin, Quantum repeaters: From quantum networks to the quantum internet, *Reviews of Modern Physics* **95**, 045006 (2023), 2212.10820.
- [51] C. H. Bennett, G. Brassard, C. Cr  peau, R. Jozsa, A. Peres, and W. K. Wootters, Teleporting an unknown quantum state via dual classical and Einstein-Podolsky-Rosen channels, *Physical Review Letters* **70**, 1895 (1993).
- [52] M.   ukowski, A. Zeilinger, M. A. Horne, and A. K. Ekert, ‘Event-ready-detectors’ Bell experiment via entanglement swapping, *Physical Review Letters* **71**, 4287 (1993).
- [53] C. H. Bennett, G. Brassard, S. Popescu, B. Schumacher, J. A. Smolin, and W. K. Wootters, Purification of Noisy Entanglement and Faithful Teleportation via Noisy Channels, *Physical Review Letters* **76**, 722 (1996).
- [54] C. H. Bennett, H. J. Bernstein, S. Popescu, and B. Schumacher, Concentrating partial entanglement by local operations, *Physical Review A* **53**, 2046 (1996).
- [55] C. H. Bennett, D. P. DiVincenzo, J. A. Smolin, and W. K. Wootters, Mixed-state entanglement and quantum error correction, *Physical Review A* **54**, 3824 (1996).
- [56] P.-S. Yan, L. Zhou, W. Zhong, and Y.-B. Sheng, Advances in quantum entanglement purification, *Science China Physics, Mechanics & Astronomy* **66**, 250301 (2023), 2304.12679.
- [57] T. D. Ladd, P. van Loock, K. Nemoto, W. J. Munro, and Y. Yamamoto, Hybrid quantum repeater based on dispersive CQED interactions between matter qubits and bright coherent light, *New Journal of Physics* **8**, 184 (2006), quant-ph/0610154.
- [58] M. Razavi, M. Piani, and N. L  tkenhaus, Quantum repeaters with imperfect memories: Cost and scalability, *Physical Review A* **80**, 032301 (2009).
- [59] M. Razavi, K. Thompson, H. Farmanbar, M. Piani, and N. L  tkenhaus, Physical and architectural considerations in quantum repeaters, in *Quantum Communications Realized II*, Vol. 7236, edited by Y. Arakawa, M. Sasaki, and H. Sotobayashi, International Society for Optics and Photonics (SPIE, 2009) pp. 18–30.
- [60] W. J. Munro, K. A. Harrison, A. M. Stephens, S. J. Devitt, and K. Nemoto, From quantum multiplexing to high-performance quantum networking, *Nature Photonics* **4**, 792 (2010).
- [61] Y.-B. Sheng and F.-G. Deng, Deterministic entanglement purification and complete nonlocal Bell-state analysis with hyperentanglement, *Physical Review A* **81**, 032307 (2010), 0912.0079.
- [62] Y.-B. Sheng and F.-G. Deng, One-step deterministic polarization-entanglement purification using spatial entanglement, *Physical Review A* **82**, 044305 (2010), 1008.3509.
- [63] C. Simon, H. de Riedmatten, and M. Afzelius, Temporally multiplexed quantum repeaters with atomic gases, *Physical Review A* **82**, 010304 (2010), 1007.5028.
- [64] S. Bratzik, S. Abruzzo, H. Kampermann, and D. Bru  , Quantum repeaters and quantum key distribution: The impact of entanglement distillation on the secret key rate, *Physical Review A* **87**, 062335 (2013).
- [65] Y.-B. Sheng, L. Zhou, and G.-L. Long, Hybrid entanglement purification for quantum repeaters, *Physical Review A* **88**, 022302 (2013).
- [66] N. Sinclair, E. Saglamyurek, H. Mallahzadeh, J. A. Slater, M. George, R. Ricken, M. P. Hedges, D. Oblak, C. Simon, W. Sohler, and W. Tittel, Spectral Multiplexing for Scalable Quantum Photonics using an Atomic Frequency Comb Quantum Memory and Feed-Forward Control, *Physical Review Letters* **113**, 053603 (2014), 1309.3202.
- [67] L. Zhou, W. Zhong, and Y.-B. Sheng, Purification of the residual entanglement, *Optics Express* **28**, 2291 (2020).
- [68] X.-M. Hu, C.-X. Huang, Y.-B. Sheng, L. Zhou, B.-H. Liu, Y. Guo, C. Zhang, W.-B. Xing, Y.-F. Huang, C.-F. Li, and G.-C. Guo, Long-Distance Entanglement Purification for Quantum Communication, *Physical Review Letters* **126**, 010503 (2021), 2101.07441.
- [69] P. Dhara, A. Patil, H. Krovi, and S. Guha, Subexponential rate versus distance with time-multiplexed quantum repeaters, *Physical Review A* **104**, 052612 (2021), 2105.01002.
- [70] P. Dhara, N. M. Linke, E. Waks, S. Guha, and K. P. Seshadreesan, Multiplexed quantum repeaters based on dual-species trapped-ion systems, *Physical Review A* **105**, 022623 (2022), 2105.06707.

- [71] C.-X. Huang, X.-M. Hu, B.-H. Liu, L. Zhou, Y.-B. Sheng, C.-F. Li, and G.-C. Guo, Experimental one-step deterministic polarization entanglement purification, *Science Bulletin* **67**, 593 (2022), 2110.04970.
- [72] S. Ecker, P. Sohr, L. Bulla, R. Ursin, and M. Bohmann, Remotely Establishing Polarization Entanglement Over Noisy Polarization Channels, *Physical Review Applied* **17**, 034009 (2022), 2110.04159.
- [73] T. Chakraborty, A. Dasa, H. van Brug, O. Pietx-Casas, P.-C. Wang, G. C. do Amaral, A. L. Tchebotareva, and W. Tittel, Towards a spectrally multiplexed quantum repeater, *arXiv:2205.10028* (2022).
- [74] E. A. V. Milligen, E. Jacobson, A. Patil, G. Vardoyan, D. Towsley, and S. Guha, Entanglement Routing over Networks with Time Multiplexed Repeaters, *arXiv:2308.15028* (2023).
- [75] E. Shchukin and P. van Loock, Optimal entanglement swapping in quantum repeaters, *Phys. Rev. Lett.* **128**, 150502 (2022).
- [76] F. Rozpędek, K. P. Seshadreesan, P. Polakos, L. Jiang, and S. Guha, All-photonics Gottesman-Kitaev-Preskill-qubit repeater using analog-information-assisted multiplexed entanglement ranking, *Physical Review Research* **5**, 043056 (2023).
- [77] W. J. Munro, K. Azuma, K. Tamaki, and K. Nemoto, Inside Quantum Repeaters, *IEEE Journal of Selected Topics in Quantum Electronics* **21**, 78 (2015).
- [78] S. Muralidharan, L. Li, J. Kim, N. Lütkenhaus, M. D. Lukin, and L. Jiang, Optimal architectures for long distance quantum communication, *Scientific Reports* **6**, 20463 (2016).
- [79] R. Van Meter, T. D. Ladd, W. J. Munro, and K. Nemoto, System Design for a Long-Line Quantum Repeater, *IEEE/ACM Transactions on Networking* **17**, 1002 (2009), 0705.4128.
- [80] T. Matsuo, C. Durand, and R. Van Meter, Quantum link bootstrapping using a ruleset-based communication protocol, *Physical Review A* **100**, 052320 (2019).
- [81] T. Matsuo, Simulation of a Dynamic, RuleSet-based Quantum Network, *arXiv:1908.10758* (2019).
- [82] K.-C. Chang, X. Cheng, M. C. Sarihan, A. K. Vinod, Y. S. Lee, T. Zhong, Y.-X. Gong, Z. Xie, J. H. Shapiro, F. N. C. Wong, and C. W. Wong, 648 Hilbert-space dimensionality in a biphoton frequency comb: entanglement of formation and Schmidt mode decomposition, *npj Quantum Information* **7** (2021).
- [83] Z. Xie, T. Zhong, S. Shrestha, X. Xu, J. Liang, Y.-X. Gong, J. C. Bienfang, A. Restelli, J. H. Shapiro, F. N. C. Wong, and C. W. Wong, Harnessing high-dimensional hyperentanglement through a biphoton frequency comb, *Nature Photonics* **9**, 536 (2015).
- [84] K.-C. Chang, X. Cheng, M. C. Sarihan, and C. W. Wong, Towards optimum franson interference recurrence in mode-locked singly-filtered biphoton frequency combs, *Photonics Research* **11**, 1175 (2023).
- [85] K.-C. Chang, X. Cheng, M. C. Sarihan, F. N. C. Wong, J. H. Shapiro, and C. W. Wong, High-dimensional Energy-time Entanglement Distribution via a Biphoton Frequency Comb, in *Conference on Lasers and Electro-Optics* (Optica Publishing Group, 2021).
- [86] M. C. Sarihan, K.-C. Chang, X. Cheng, Y. S. Lee, T. Zhong, H. Zhou, Z. Zhang, F. N. Wong, J. H. Shapiro, and C. W. Wong, High dimensional quantum key distribution with biphoton frequency combs through energy-time entanglement, in *Conference on Lasers and Electro-Optics* (OSA, 2019).
- [87] X. Cheng, M. C. Sarihan, K.-C. Chang, C. Chen, F. N. C. Wong, and C. W. Wong, Secure high dimensional quantum key distribution based on wavelength-multiplexed time-bin encoding, in *Conference on Lasers and Electro-Optics* (Optica Publishing Group, 2021).
- [88] M. C. Sarihan, X. Cheng, K.-C. Chang, and C. W. Wong, Wavelength-multiplexed multi-user quantum network based on high-dimensional time-bin encoding, in *CLEO 2023* (Optica Publishing Group, 2023).
- [89] R.-R. Meng, X. Liu, M. Jin, Z.-Q. Zhou, C.-F. Li, and G.-C. Guo, Solid-state quantum nodes based on color centers and rare-earth ions coupled with fiber fabry-pérot microcavities, *Chip*, 100081 (2024).
- [90] Y. Lei, F. Kimiaee Asadi, T. Zhong, A. Kuzmich, C. Simon, and M. Hosseini, Quantum optical memory for entanglement distribution, *Optica* **10**, 1511 (2023).
- [91] K. Goodenough, S. de Bone, V. L. Addala, S. Krastanov, S. Jansen, D. Gijswijt, and D. Elkouss, Near-term  $n$  to  $k$  distillation protocols using graph codes, *arXiv:2303.11465* (2023).
- [92] P. K. Sarvepalli, A. Klappenecker, and M. Rötteler, Asymmetric quantum codes: constructions, bounds and performance, *Proceedings of the Royal Society A: Mathematical, Physical and Engineering Sciences* **465**, 1645 (2009), <https://www.jstor.org/stable/30243785>.
- [93] J. Ghosh, A. G. Fowler, and M. R. Geller, Surface code with decoherence: An analysis of three superconducting architectures, *Physical Review A* **86**, 062318 (2012), 1210.5799.
- [94] S. Ourari, I. Dusanowski, S. P. Horvath, M. T. Uysal, C. M. Phenicie, P. Stevenson, M. Raha, S. Chen, R. J. Cava, N. P. de Leon, and J. D. Thompson, Indistinguishable telecom band photons from a single Er ion in the solid state, *Nature* **620**, 977 (2023).



### Appendix A: Noise model and decoherence

We consider the following Pauli channel noise model for qubit decoherence [92, 93]:

$$\mathcal{N}_{m_1^\star, m_2^\star}(\rho) = p_I \rho + p_X X \rho X + p_Y Y \rho Y + p_Z Z \rho Z, \quad (\text{A1})$$

where  $X, Y, Z$  are the single-qubit Pauli operators, defined as

$$X := \begin{pmatrix} 0 & 1 \\ 1 & 0 \end{pmatrix}, \quad Y := \begin{pmatrix} 0 & -i \\ i & 0 \end{pmatrix}, \quad Z := \begin{pmatrix} 1 & 0 \\ 0 & -1 \end{pmatrix}, \quad (\text{A2})$$

and the probabilities  $p_I, p_X, p_Y, p_Z$  are defined as

$$p_I = \frac{1 + e^{-\frac{1}{m_2^\star}}}{2} - \frac{1 - e^{-\frac{1}{m_1^\star}}}{4}, \quad (\text{A3})$$

$$p_X = \frac{1 - e^{-\frac{1}{m_1^\star}}}{4}, \quad (\text{A4})$$

$$p_Y = \frac{1 - e^{-\frac{1}{m_1^\star}}}{4}, \quad (\text{A5})$$

$$p_Z = \frac{1 - e^{-\frac{1}{m_2^\star}}}{2} - \frac{1 - e^{-\frac{1}{m_1^\star}}}{4}, \quad (\text{A6})$$

where  $m_1^\star, m_2^\star \in \{1, 2, \dots\}$ . This channel is the Pauli-twirled version of the concatenated amplitude damping and dephasing channels.

Let us also define the two-qubit Bell states as follows:

$$|\Phi^\pm\rangle := \frac{1}{\sqrt{2}}(|0, 0\rangle \pm |1, 1\rangle), \quad \Phi^\pm := |\Phi^\pm\rangle\langle\Phi^\pm|, \quad (\text{A7})$$

$$|\Psi^\pm\rangle := \frac{1}{\sqrt{2}}(|0, 1\rangle \pm |1, 0\rangle), \quad \Psi^\pm := |\Psi^\pm\rangle\langle\Psi^\pm|. \quad (\text{A8})$$

*Decoherence of an entangled qubit pair.* Now, let us suppose that the initial state of an entangled qubit pair is the perfect maximally-entangled Bell state  $\Phi^+$ . Then, after  $m \in \{1, 2, 3, \dots\}$  time steps, it is straightforward to show that the decohered entangled state is equal to

$$\begin{aligned} & (\mathcal{N}_{m_1^\star, m_2^\star} \otimes \mathcal{N}_{m_1^\star, m_2^\star})^{\circ m}(\Phi^+) \\ &= \frac{1}{4} \left( (1 + e^{-2m/m_1^\star} + 2e^{-2m/m_2^\star})\Phi^+ \right. \\ & \quad + (1 + e^{-2m/m_1^\star} - 2e^{-2m/m_2^\star})\Phi^- \\ & \quad + (1 - e^{-2m/m_1^\star})\Psi^+ \\ & \quad \left. + (1 - e^{-2m/m_1^\star})\Psi^- \right). \end{aligned} \quad (\text{A9})$$

For a proof, we refer to Ref. [43, Appendix E]. This implies that the fidelity of the state after  $m$  time steps is  $\frac{1}{4}(1 + e^{-2m/m_1^\star} + 2e^{-2m/m_2^\star})$ .

In order to connect with the results presented in the main text, for a given value of  $m^\star$  as presented in the main text, let us take

$$m_1^\star = 2m^\star, \quad m_2^\star = 2m^\star. \quad (\text{A10})$$

In other words, we consider equal dephasing and amplitude damping. The fidelity after  $m$  time steps is then equal to

$$f(m) = \frac{1}{4}(1 + 3e^{-\frac{m}{m^\star}}). \quad (\text{A11})$$

Note that we have chosen the value of  $m_2^\star$  in Eq. (A10) such that, at the cutoff time  $m^\star$ , the fidelity of the entangled qubit pair is  $f(m^\star) = \frac{1}{4}(1 + 3/e) \approx 0.5259$ . We emphasize that our results can be applied to other choices of  $m_1^\star$  and  $m_2^\star$ —in particular, choices that could take dephasing as the dominant source of noise [94] or in order to make connections to prior works [20, 23, 30, 41, 58].

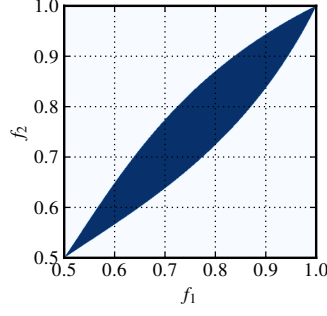


FIG. 17. Usefulness of distillation with the BBPSSW protocol [53]. The dark blue shaded region indicates the values of the initial fidelities,  $f_1$  and  $f_2$ , for which the fidelity after distillation exceeds the fidelity of the best of the two links, i.e., when  $F_{\text{distill}}(f_1, f_2) \geq \max\{f_1, f_2\}$ .

We can invert the fidelity function in Eq. (A11), such that for a given fidelity  $F$ , the corresponding age of the qubits is given by

$$f^{-1}(F) = \lceil -m^* \log((4F - 1)/3) \rceil, \quad (\text{A12})$$

for all  $F \in (f(m^*), 1)$ , where we take the ceiling  $\lceil \cdot \rceil$  because we want an integer for the age.

We also remark that the decohered entangled state in Eq. (A9) is a Bell-diagonal state of the form

$$(a + b)\Phi^+ + (a - b)\Phi^- + c\Psi^+ + c\Psi^-. \quad (\text{A13})$$

As such, its entanglement can be characterized entirely by the quantity  $a + b$ , namely, the fidelity of the state with respect to  $\Phi^+$ . In particular, the state is entangled if and only if this fidelity is strictly greater than  $\frac{1}{2}$ ; see, e.g., [28, Chapter 2]. Therefore, under the assumptions in Eq. (A10), such that the fidelity is given by Eq. (A11), we find that the state in Eq. (A9) is entangled for all time steps  $m \in \{0, 1, 2, \dots, m^*\}$ . Furthermore, inserting  $F = \frac{1}{2}$  in Eq. (A12), we find that the age at which entanglement is lost is  $\lceil m^* \log(3) \rceil$ .

## Appendix B: Entanglement distillation with the BBPSSW protocol

In this work, the entanglement distillation protocol we consider is the BBPSSW protocol introduced in Ref. [53]. This protocol, involving the distillation of two entangled pairs to one, consists of a CNOT gate applied locally to each pair of qubits, followed by measuring the local target qubits of the CNOTs in the Pauli-Z basis. If  $f_1$  and  $f_2$  are the fidelities of the two entangled qubit pairs, then the success probability of the distillation procedure is

$$P_{\text{distill}}(f_1, f_2) = \frac{8}{9}f_1f_2 - \frac{2}{9}(f_1 + f_2) + \frac{5}{9}, \quad (\text{B1})$$

and the fidelity of the resulting state is

$$F_{\text{distill}}(f_1, f_2) = \frac{1}{P_{\text{distill}}(f_1, f_2)} \left( \frac{10}{9}f_1f_2 - \frac{1}{9}(f_1 + f_2) + \frac{1}{9} \right) \quad (\text{B2})$$

$$= \frac{1 - (f_1 + f_2) + 10f_1f_2}{5 - 2(f_1 + f_2) + 8f_1f_2}. \quad (\text{B3})$$

With this expression for the fidelity after entanglement distillation, if we let  $f_1 = f(m_1)$  and  $f_2 = f(m_2)$ , with  $m_1$  and  $m_2$  the ages of the two entangled states, then we can calculate the updated age as  $m' = f^{-1}(F_{\text{distill}}(f(m_1), f(m_2)))$ , with the expression for  $f^{-1}$  given in Eq. (A12). In particular, the updated age  $m'$  is given by:

$$m' = \left\lceil m^* \log \left( \frac{15 - 6(f(m_1) + f(m_2)) + 24f(m_1)f(m_2)}{32f(m_1)f(m_2) - 2(f(m_1) + f(m_2)) - 1} \right) \right\rceil. \quad (\text{B4})$$

Now, distillation should be considered useful only when it can improve upon the fidelity of the best of the two links. In other words, in order for distillation to be useful, we should have  $F_{\text{distill}}(f_1, f_2) > \max\{f_1, f_2\}$ . In Fig. 17, we plot the  $(f_1, f_2)$  region defined by this inequality.

### 1. The pumping policy

Let us recall that the fidelity of the pumping policy after  $r \in \{1, 2, \dots\}$  rounds is defined by the recurrence relation  $f_r = F_{\text{distill}}(f_{r-1}, f_0)$ , where  $f_0$  is the initial fidelity. Using Eq. (B3), we can write this recurrence relation as

$$f_r = \frac{a_1 f_{r-1} + a_2}{a_3 f_{r-1} + a_4}, \quad a_1 := 10f_0 - 1, \quad a_2 := 1 - f_0, \quad a_3 := 8f_0 - 2, \quad a_4 := 5 - 2f_0. \quad (\text{B5})$$

In this section, we provide a closed-form, analytical solution to this recurrence relation.

**Lemma 1.** Define the matrix  $A := \begin{pmatrix} a_1 & a_2 \\ a_3 & a_4 \end{pmatrix}$ , where  $a_1, a_2, a_3, a_4$  are defined in Eq. (B5). For  $r \in \{1, 2, \dots\}$ , consider the vector

$$\vec{v}_r = \begin{pmatrix} v_{r,0} \\ v_{r,1} \end{pmatrix} := A^r \vec{v}_0, \quad \vec{v}_0 = \begin{pmatrix} f_0 \\ 1 \end{pmatrix}. \quad (\text{B6})$$

It holds that  $f_r = \frac{v_{r,0}}{v_{r,1}}$ .

*Proof.* We prove this by induction on  $r$ . For the base case of  $r = 1$ , we have

$$\begin{pmatrix} v_{1,0} \\ v_{1,1} \end{pmatrix} = \begin{pmatrix} a_1 & a_2 \\ a_3 & a_4 \end{pmatrix} \begin{pmatrix} f_0 \\ 1 \end{pmatrix} = \begin{pmatrix} a_1 f_0 + a_2 \\ a_3 f_0 + a_4 \end{pmatrix}, \quad (\text{B7})$$

which is consistent with Eq. (B5). Now, the induction step: assuming that the result holds for  $r \in \{1, 2, \dots\}$ , using Eq. (B5) we obtain

$$f_{r+1} = \frac{a_1 f_r + a_2}{a_3 f_r + a_4} \quad (\text{B8})$$

$$= \frac{a_1 \frac{v_{r,0}}{v_{r,1}} + a_2}{a_3 \frac{v_{r,0}}{v_{r,1}} + a_4} \quad (\text{B9})$$

$$= \frac{a_1 v_{r,0} + a_2 v_{r,1}}{a_3 v_{r,0} + a_4 v_{r,1}}. \quad (\text{B10})$$

From this, we see that

$$\begin{pmatrix} a_1 v_{r,0} + a_2 v_{r,1} \\ a_3 v_{r,0} + a_4 v_{r,1} \end{pmatrix} = \begin{pmatrix} a_1 & a_2 \\ a_3 & a_4 \end{pmatrix} \begin{pmatrix} v_{r,0} \\ v_{r,1} \end{pmatrix} \quad (\text{B11})$$

$$= A \cdot A^r \vec{v}_0 \quad (\text{B12})$$

$$= A^{r+1} \vec{v}_0 \quad (\text{B13})$$

$$= \vec{v}_{r+1}, \quad (\text{B14})$$

which means that  $f_{r+1} = \frac{v_{r+1,0}}{v_{r+1,1}}$ . This completes the proof. ■

**Theorem 1.** The fidelity after  $r \in \{1, 2, \dots\}$  rounds of the pumping policy is given by  $f_r = \frac{\alpha_r}{\beta_r}$ , where

$$\begin{aligned} \alpha_r = & -(1 - 4f_0 + 6f_0^2) \left( \left( 2 + 4f_0 - \sqrt{7 - 26f_0 + 28f_0^2} \right)^r - \left( 2 + 4f_0 + \sqrt{7 - 26f_0 + 28f_0^2} \right)^r \right) \\ & + f_0 \sqrt{7 - 26f_0 + 28f_0^2} \left( \left( 2 + 4f_0 - \sqrt{7 - 26f_0 + 28f_0^2} \right)^r + \left( 2 + 4f_0 + \sqrt{7 - 26f_0 + 28f_0^2} \right)^r \right), \end{aligned} \quad (\text{B15})$$

$$\begin{aligned} \beta_r = & -(3 - 8f_0 + 8f_0^2) \left( \left( 2 + 4f_0 - \sqrt{7 - 26f_0 + 28f_0^2} \right)^r - \left( 2 + 4f_0 + \sqrt{7 - 26f_0 + 28f_0^2} \right)^r \right) \\ & + \sqrt{7 - 26f_0 + 28f_0^2} \left( \left( 2 + 4f_0 - \sqrt{7 - 26f_0 + 28f_0^2} \right)^r + \left( 2 + 4f_0 + \sqrt{7 - 26f_0 + 28f_0^2} \right)^r \right). \end{aligned} \quad (\text{B16})$$

*Proof.* We start with the eigenvalues and eigenvectors of the matrix  $A = \begin{pmatrix} a_1 & a_2 \\ a_3 & a_4 \end{pmatrix}$ . The eigenvalues  $\lambda_{\pm}$  and corresponding eigenvectors  $\vec{x}_{\pm}$  are readily found to be

$$\lambda_{\pm} = 2 + 4f_0 \pm \sqrt{7 - 26f_0 + 28f_0^2}, \quad (\text{B17})$$

$$\vec{x}_{\pm} = \begin{pmatrix} \omega_{\pm} \\ 1 \end{pmatrix}, \quad \omega_{\pm} = \frac{-3 + 6f_0 \pm \sqrt{7 - 26f_0 + 28f_0^2}}{-2 + 8f_0}. \quad (\text{B18})$$

In particular, we have that  $A\vec{x}_{\pm} = \lambda_{\pm}\vec{x}_{\pm}$ . Then, the initial vector  $\vec{v}_0 = \begin{pmatrix} f_0 \\ 1 \end{pmatrix}$  can be expressed in terms of the eigenvectors  $\vec{x}_{\pm}$  as

$$\vec{v}_0 = \begin{pmatrix} f_0 \\ 1 \end{pmatrix} = c_1\vec{x}_+ + c_2\vec{x}_-, \quad c_1 = \frac{f_0 - \omega_-}{\omega_+ + \omega_-}, \quad c_2 = 1 - c_1. \quad (\text{B19})$$

We therefore find that

$$\vec{v}_r = A^r \vec{v}_0 \quad (\text{B20})$$

$$= c_1 A^r \vec{x}_+ + c_2 A^r \vec{x}_- \quad (\text{B21})$$

$$= c_1 \lambda_+^r \vec{x}_+ + c_2 \lambda_-^r \vec{x}_- \quad (\text{B22})$$

$$= c_1 \lambda_+^r \begin{pmatrix} \omega_+ \\ 1 \end{pmatrix} + c_2 \lambda_-^r \begin{pmatrix} \omega_- \\ 1 \end{pmatrix}, \quad (\text{B23})$$

which implies (via Lemma 1) that

$$f_r = \frac{c_1 \lambda_+^r \omega_+ + c_2 \lambda_-^r \omega_-}{c_1 \lambda_+^r + c_2 \lambda_-^r} = \frac{\lambda_-^r \omega_- + c_1 (\lambda_+^r \omega_+ - \lambda_-^r \omega_-)}{\lambda_-^r + c_1 (\lambda_+^r - \lambda_-^r)}. \quad (\text{B24})$$

After substitution and much simplification, we obtain the desired expressions in Eq. (B15) and Eq. (B16). ■

**Corollary 2.** For the sequence  $\{f_r\}_r$  of fidelities defined by the pumping policy, it holds that

$$\lim_{r \rightarrow \infty} f_r = \frac{-3 + 6f_0 + \sqrt{7 - 26f_0 + 28f_0^2}}{-2 + 8f_0}. \quad (\text{B25})$$

*Proof.* We can write the expression for  $f_r$  in Eq. (B24) as

$$f_r = \frac{\left(\frac{\lambda_-}{\lambda_+}\right)^r \omega_- + c_1 \left(\omega_+ - \left(\frac{\lambda_-}{\lambda_+}\right)^r \omega_-\right)}{\left(\frac{\lambda_-}{\lambda_+}\right)^r + c_1 \left(1 - \left(\frac{\lambda_-}{\lambda_+}\right)^r\right)}. \quad (\text{B26})$$

Now, it is straightforward to see that  $\lambda_{\pm} \geq 0$  for all  $f_0 \in [\frac{1}{2}, 1]$ , and furthermore that  $\lambda_+ > \lambda_-$ . Therefore,  $\frac{\lambda_-}{\lambda_+} \in [0, 1)$ , which means that  $\lim_{r \rightarrow \infty} \left(\frac{\lambda_-}{\lambda_+}\right)^r = 0$ . We therefore find that  $\lim_{r \rightarrow \infty} f_r = \omega_+$ , and because  $\omega_+$  (defined in Eq. (B18)) is precisely the expression on the right-hand side of Eq. (B25), we have the desired result. ■

## 2. Banding vs. pumping

To gain an understanding of the difference between the banding and pumping policies of entanglement distillation, we consider here a three-node chain with  $n_{ch}$  channels between the nodes. In this setting, by the SWAP-DISTILL policy, we mean that all  $n_{ch}$  links are active at the same time, entanglement swapping is performed on all of them and we assume that they all succeed, and then all of the end-to-end links are distilled into one end-to-end link. By the DISTILL-SWAP policy, we mean that all  $n_{ch}$  on both sides are distilled into one link, and then entanglement swapping is performed on them and assumed to be successful.

Let us first consider the banding approach to distillation, as defined above. Once all  $n_{ch}$  links are put in pairs, a first round of  $\frac{n_{ch}}{2}$  distillation attempts are made; the resulting links are all of the same fidelity, and they are paired again. In the next round,  $\frac{n_{ch}}{4}$  distillation attempts are made, and the process continues until we have one link remaining. Thus a total number of  $\log_2(n)$  rounds are needed (supposing that  $n_{ch}$  is a power of two).



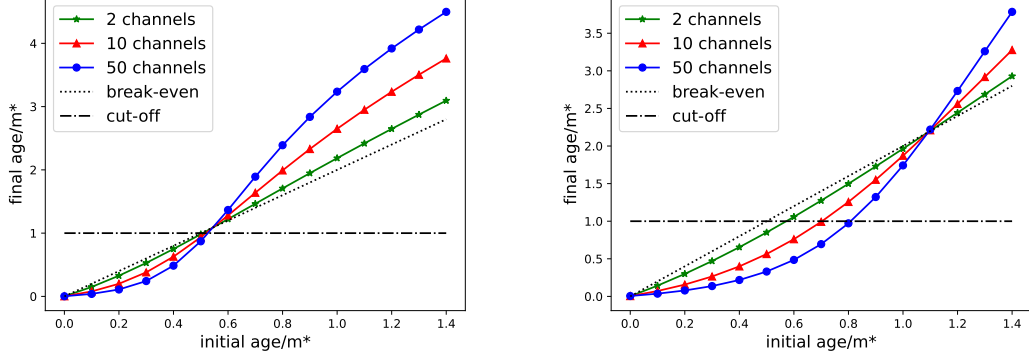


FIG. 18. Comparison of the SWAP-DISTILL (top) and DISTILL-SWAP (bottom) policies for a three-node chain with  $n_{ch}$  links connecting the neighboring nodes, as described in Sec. B 2. Here we use the banded policy to perform distillation. The SWAP-DISTILL policy is not useful beyond initial age  $m^*/2$ , whereas DISTILL-SWAP can extend this threshold to  $m^*$ .

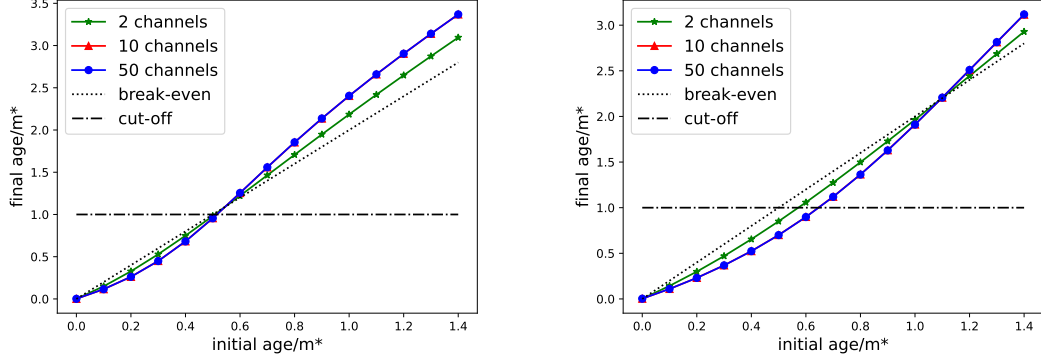


FIG. 19. Comparison of the SWAP-DISTILL (top) and DISTILL-SWAP (bottom) policies for a three-node chain with  $n_{ch}$  links connecting the neighboring nodes, as described in Sec. B 2. Now, instead of the banding policy, we use the pumping policy for distillation. As with banded purification, SWAP-DISTILL is not useful beyond an initial age of  $m^*/2$ , whereas DISTILL-SWAP can extend this threshold, but now not quite up to  $\approx m^*$ . This is a consequence of the fact that the pumping policy has a strict limit on the fidelity that can be achieved with an increasing number of channels, as shown in Eq. (5).

Results for the banding approach are shown in Fig. 18. We see that in the case of SWAP-DISTILL, the cut-off of  $m^*$  is breached by the end-to-end link if the initial links are older than  $\approx 0.5m^*$ . This is so because distillation is not useful for links of age greater than the cut-off  $m^*$ , and swapping adds the ages of links. In the case of DISTILL-SWAP, the threshold is higher and equal to  $m^*$ , because distillation occurs first. More importantly, we note that in both cases these thresholds are independent of the number of distillation channels used, indicated by the intersection of the different curves. On the other hand, for links of age below the threshold, using an increasing number of links, an arbitrarily high fidelity link can be obtained.

All of the analysis above was done considering a idealised situation in which links of the same age are available always for distillation. This is of course not necessarily true in practice. In practical settings, links will have to be used as and when they are produced. Therefore, it is important to look also at the previously mentioned pumping policy.

Results for the pumping policy are shown in Fig. 19. Although the trends remain very similar to Fig. 18, one important difference is noticeable immediately. When the pumping policy is used for distillation, the final age of the distilled link always saturates to a value approaching the limit in Eq. (5) as the number of channels increases. This can be seen by the convergence of the red (triangle) and blue (circle) curves for  $n_{ch} = 10$  and  $n_{ch} = 50$ , respectively. This is in contrast to the observations in Fig. 18, in which we observe that increasing the number of channels progressively decreases the final age.

### Appendix C: Distill-swap vs swap-distill policy: analytical results

Here we analytically compare the performance of the DISTILL-SWAP and SWAP-DISTILL policies in the case of three nodes. To simplify the analysis, we restrict ourselves to the cases with two and four channels, and consider all elementary links to be active simultaneously with the same fidelity. The general result for an arbitrary number of channels is difficult to calculate analytically given the large number of possible trajectories that can lead to the successful generation of at least one end-to-end link. Seeing in Appendix B 2 that the banded policy performs better than pumping, in this section we look exclusively at the banded policy. The performance of the policies is evaluated by the success probability of establishing at least one end-to-end entangled link and by the average fidelity of an end-to-end link.

#### 1. Two-channel case

Let  $f_0$  be the initial fidelity of both the active links on each side given in terms of the initial age  $m_0$  according to Eq. (A11) as  $f_0 = f(m_0) = \frac{1}{4}(1 + 3e^{-m_0/m^*})$ . Let us first consider the DISTILL-SWAP policy. The probability of distillation being successful simultaneously on both sides followed by a successful entanglement swapping of the distilled links is given by

$$p_{ds} = p_{sw}p_d^2 = p_{sw}((8f_0^2 - 4f_0 + 5)/9)^2, \quad (C1)$$

where  $p_d = (8f_0^2 - 4f_0 + 5)/9$  is the success probability of one distillation attempt, as given by Eq. (B1). The fidelity and ages of the successfully distilled links on both sides is given by

$$f_d = (1 - 2f_0 + 10f_0^2)/(5 - 4f_0 + 8f_0^2), \quad (C2)$$

$$m_d = \lceil -m^* \log((4f_d - 1)/3) \rceil. \quad (C3)$$

Finally, the age of virtual link produced by swapping is the sum of the ages of the elementary links consumed, i.e.,  $2m_d$ . Therefore, the fidelity of the end-to-end link is given by:

$$f_{ds} = \frac{1}{4}(1 + 3e^{-2m_d/m^*}). \quad (C4)$$

Next, we consider the SWAP-DISTILL policy. For this policy, two cases may arise depending on the number of successful entanglement swaps. Let  $p_{sd}^{(1)}, f_{sd}^{(1)}$  and  $p_{sd}^{(2)}, f_{sd}^{(2)}$  be the success probability and fidelity, respectively, of the two cases. The two cases are based on whether one or both of the entanglement swaps succeed. Then, the total probability of producing at least one end-to-end link is the sum of two cases and is given by

$$p_{sd} = p_{sd}^{(1)} + p_{sd}^{(2)}, \quad (C5)$$

and the weighted (expected) fidelity of the final distilled virtual link produced is given by

$$f_{sd} = \frac{p_{sd}^{(1)}f_{sd}^{(1)} + p_{sd}^{(2)}f_{sd}^{(2)}}{p_{sd}^{(1)} + p_{sd}^{(2)}}. \quad (C6)$$

Let us now determine analytical expressions for  $p_{sd}^{(1)}, f_{sd}^{(1)}, p_{sd}^{(2)}, f_{sd}^{(2)}$ .

1. Both entanglement swaps succeed. In this case, the probability that both entanglement swaps succeed, followed by a successful distillation attempt, is given by

$$p_{sd}^{(2)} = p_{sw}^2(8f_s^2 - 4f_s + 5)/9, \quad (C7)$$

where the “(2)” in the superscript of  $p_{sd}^{(2)}$  indicates the number of successful swaps and  $f_s$  is the fidelity of the virtual links produced after successful swapping, given by

$$f_s = \frac{1}{4}(1 + 3e^{-\frac{2m_0}{m^*}}). \quad (C8)$$

The resulting fidelity, after distillation, is then

$$f_{sd}^{(2)} = F_{\text{distill}}(f_s, f_s) = \frac{1 - 2f_s + 10f_s^2}{5 - 4f_s + 8f_s^2}. \quad (C9)$$

- Only one entanglement swap is successful. This can happen in two ways, therefore the probability of successfully producing one end-to-end link in this case is simply given by

$$p_{sd}^{(1)} = 2p_{sw}(1 - p_{sw}), \quad (\text{C10})$$

because no distillation can be performed in this case, which also means that

$$f_{sd}^{(1)} = f_s, \quad (\text{C11})$$

with  $f_s$  as defined in Eq. (C8).

## 2. Four-channel case

Now, for the four-channel case, let us start with the DISTILL-SWAP policy. Recall that under the banding policy, at most three rounds of distillation can be performed with four links. Based on this, there are three trajectories can lead to one end-to-end link, and the corresponding success probabilities and fidelities are derived below. We combine them to obtain the total probability and weighted (expected) fidelity of an end-to-end link, in a manner analogous to (C5) and (C6). Throughout these derivations, we let  $f_0$  be the initial fidelity of all links, we let  $p_d \equiv P_{\text{distill}}(f_0, f_0)$  and  $f_d \equiv F_{\text{distill}}(f_0, f_0)$  be the success probability and fidelity, respectively, after the first round of distillation. Similarly, we let  $p_{d_2} \equiv P_{\text{distill}}(f_d, f_d)$  and  $f_{d_2} \equiv F_{\text{distill}}(f_d, f_d)$  be the success probability and fidelity, respectively, after the second round of distillation. The corresponding ages of the links after each round are denoted by  $m_d \equiv f^{-1}(f_d)$  and  $m_{d_2} \equiv f^{-1}(f_{d_2})$ , where we recall the function  $f(m) = \frac{1}{4}(1 + 3 \exp(-m/m^*))$  and its inverse  $f^{-1}(F) = \lceil -m^* \log((4F - 1)/3) \rceil$ .

- Only one pair of links is distilled successfully on each side, and the distilled link is successfully swapped. There are four possible ways this can occur, which means that the success probability and resulting fidelity in this case are given by

$$p_{ds}^{(1,1)} = p_{sw}(4p_d^2(1 - p_d)^2), \quad (\text{C12})$$

$$f_{ds}^{(1,1)} = \frac{1}{4} \left( 1 + 3 \exp \left( -\frac{2m_d}{m^*} \right) \right), \quad (\text{C13})$$

where the “(1, 1)” in the superscript denotes that only one distillation attempt succeeded on each side.

- All three distillation attempts succeed on one side and only one distillation attempt succeeds on the other side, followed by a successful entanglement swapping. (Note that the case of only two distillation successes on either side does not lead to an active link, and thus entanglement swapping to generate an end-to-end link is not possible.) This can happen in four ways - two ways to choose which side all three distillation will succeed and when all attempts succeed on one side, either the first or the second attempt could fail on the other side. Denoting the corresponding success probability and fidelity by  $p_{ds}^{(3,1)}$  and  $f_{ds}^{(3,1)}$ , respectively, we have

$$p_{ds}^{(3,1)} = p_{sw}(4p_d^3(1 - p_d)p_{d_2}), \quad (\text{C14})$$

$$f_{ds}^{(3,1)} = \frac{1}{4} \left( 1 + 3 \exp \left( -\frac{m_d + m_{d_2}}{m^*} \right) \right). \quad (\text{C15})$$

- All three distillation attempts succeed on both sides, followed by successful entanglement swapping. In this case, denoting the success probability and fidelity by  $p_{ds}^{(3,3)}$  and  $f_{ds}^{(3,3)}$ , respectively, we have

$$p_{ds}^{(3,3)} = p_{sw}(p_d^2 p_{d_2})^2, \quad (\text{C16})$$

$$f_{ds}^{(3,3)} = \frac{1}{4} \left( 1 + 3 \exp \left( -\frac{2m_{d_2}}{m^*} \right) \right). \quad (\text{C17})$$

Therefore, the total success probability of producing at least one end-to-end link is given by

$$p_{ds} = p_{ds}^{(1,1)} + p_{ds}^{(3,1)} + p_{ds}^{(3,3)}, \quad (\text{C18})$$

and the expected fidelity is given by

$$f_{ds} = \frac{f_{ds}^{(1,1)} p_{ds}^{(1,1)} + f_{ds}^{(3,1)} p_{ds}^{(3,1)} + f_{ds}^{(3,3)} p_{ds}^{(3,3)}}{p_{ds}^{(1,1)} + p_{ds}^{(3,1)} + p_{ds}^{(3,3)}}. \quad (C19)$$

Next, we move to the SWAP-DISTILL policy. In this case, six trajectories can lead to a successful end-to-end link generation. They are listed below.

1. Only one entanglement swapping attempt succeeds, and thus no distillation is possible. There are  $\binom{4}{1} = 4$  possible pairings for the entanglement swapping, which means that the success probability  $p_{sd}^{(1)}$  and the fidelity  $f_{sd}^{(1)}$  are given by

$$p_{sd}^{(1)} = 4p_{sw}(1 - p_{sw})^3, \quad (C20)$$

$$f_{sd}^{(1)} = f_s \equiv f(2m_0) = \frac{1}{4} \left( 1 + 3 \exp \left( -\frac{2m_0}{m^*} \right) \right). \quad (C21)$$

2. Two entanglement swapping attempts succeed, and then one distillation attempt is made and succeeds. There are now  $\binom{4}{2} = 6$  possible ways to obtain two successful entanglement swaps, which means the the success probability  $p_{sd}^{(2)}$  and fidelity  $f_{sd}^{(2)}$  in the case are given by

$$p_{sd}^{(2)} = 6p_{sw}^2(1 - p_{sw})^2 p_s, \quad (C22)$$

$$f_{sd}^{(2)} = F_{\text{distill}}(f_s, f_s) = (1 - 2f_s + 10f_s^2)/(5 - 4f_s + 8f_s^2), \quad (C23)$$

where  $p_s \equiv P_{\text{succ}}(f_s, f_s) = (8f_s^2 - 4f_s + 5)/9$  is the success probability of distilling two virtual links of age  $2m_0$  (the fidelity is  $f_s = f(2m_0)$ , as defined in Eq. (C21)).

3. If three entanglement swaps succeed (can happen in  $\binom{4}{3} = 4$  ways), then two distillation attempts need to be made in order to get one end-to-end link. Two sub-cases arise

(a) The first distillation attempt may fail leaving us with just one end-to-end link.

(b) Both distillation attempts might succeed.

Thus, the success probability and fidelity is a sum (and weighted sum) of these two sub-cases, and is given by:

$$p_{sd}^{(3)} = 4p_{sw}^3(1 - p_{sw})(1 - p_s) + 4p_{sw}^3(1 - p_{sw}p_s p_{s2}), \quad (C24)$$

$$f_{sd}^{(3)} = \frac{1}{p_{sd}^{(3)}} \left( 4p_{sw}^3(1 - p_{sw})(1 - p_s)f_s + 4p_{sw}^3(1 - p_{sw}p_s p_{s2}) \frac{1 - (f_s + f_{sd}^{(2)}) + 10f_s f_{sd}^{(2)}}{5 - 2(f_s + f_{sd}^{(2)}) + 8f_s f_{sd}^{(2)}} \right) \quad (C25)$$

where  $p_{s2} = (8f_s f_{sd}^{(2)} - 2(f_s + f_{sd}^{(2)}) + 5)/9$  is the distillation success probability for two links, one with age  $2m_0$  and fidelity  $f_s$  and another which has been obtained by distilling two links of age  $2m_0$  and thus having fidelity  $f_{sd}^{(2)}$ .

4. Case 4: All 4 entanglement swapping attempts succeed. Again two sub-cases arise—one where all three subsequent distillation attempts succeed, and second where the one of the two first round of distillation attempts fail (can happen in two ways), and there is no scope to distill further. Thus, the success probability and fidelity is a sum (and weighted sum) of these two sub-cases, and is given by:

$$p_{sd}^{(4)} = p_{sw}^4 p_s^2 p_{s3} + 2p_{sw}^4 p_s(1 - p_s), \quad (C26)$$

$$f_{sd}^{(4)} = \frac{1}{p_{sd}^{(4)}} \left( p_{sw}^4 p_s^2 p_{s3} (1 - 2f_{sd}^{(2)} + 10 * (f_{sd}^{(2)})^2) / (5 - 4f_{sd}^{(2)} + 8(f_{sd}^{(2)})^2) + 2p_{sw}^4 p_s(1 - p_s) f_s^{(2)} \right), \quad (C27)$$

where  $p_{s3} = ((8f_{sd}^{(2)})^2 - 4f_{sd}^{(2)} + 5)/9$



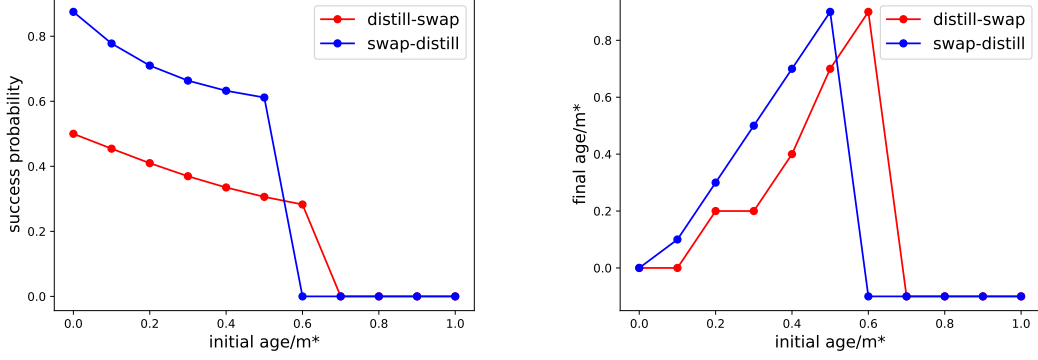


FIG. 20. Comparison of the DISTILL-SWAP and SWAP-DISTILL policies for a three-node chain with four channels connecting the neighboring nodes, as described in Sec. C. We look at the probability of successfully producing at least one end-to-end entangled link (top) and the average age of that link (when successfully produced) (bottom). For distillation, we use the banded policy. We see again that the SWAP-DISTILL policy is not useful beyond an initial age of  $m^*/2$ , whereas DISTILL-SWAP can extend this threshold up to  $m^*$  by using an increasing number of channels.

Therefore, the total success probability of getting an end-to-end entangled link and the final fidelity of the link when SWAP-DISTILL policy is used is given by:

$$\begin{aligned}
 p_{sd} &= 4p_{sw}(1-p_{sw})^3 + 6p_{sw}^2(1-p_{sw})^2p_s + 4p_{sw}^3(1-p_{sw})(1-p_s) + 4p_{sw}^3(1-p_{sw}p_s p_{s2}) + p_{sw}^4p_s^2p_{s3} + 2p_{sw}^4p_s(1-p_s), \\
 f_{sd} &= \frac{1}{p_{sd}} \left( p_{sw}(1-p_{sw})^3 f_s + 6p_{sw}^2(1-p_{sw})^2 p_s f_{sd}^{(2)} + (4p_{sw}^3(1-p_{sw})(1-p_s) f_s \right. \\
 &\quad \left. + 4p_{sw}^3(1-p_{sw}p_s p_{s2}) \frac{1 - (f_s + f_{sd}^{(2)}) + 10f_s f_{sd}^{(2)}}{5 - 2(f_s + f_{sd}^{(2)}) + 8f_s f_{sd}^{(2)}} + p_{sw}^4p_s^2p_{s3} \frac{1 - 2f_{sd}^{(2)} + 10(f_{sd}^{(2)})^2}{5 - 4f_{sd}^{(2)} + 8(f_{sd}^{(2)})^2} + 2p_{sw}^4p_s(1-p_s) f_{sd}^{(2)} \right) \quad (C28)
 \end{aligned}$$

In Fig. 20, we show the results for four channels. It is clear from Fig. 20 that SWAP-DISTILL has a higher probability of success compared to DISTILL-SWAP when the initial age of the links is less than  $m^*/2$ , beyond which it fails to succeed. Unlike distillation, success probability of entanglement swapping is independent of the quality of the used links. This is the primary reason for an asymmetry in the success rates of SWAP-DISTILL and DISTILL-SWAP policies. The probability of at least one entanglement swap being successful increases exponentially with the number of attempts available, whereas the probability of all distillations being successful falls with an increasing number of attempts, irrespective of the ages of the links involved. Thus, it is clear that if the aim is to generate at least one end-to-end link as quickly as possible, i.e., if the aim is to minimize waiting time, the SWAP-DISTILL is the policy of choice. At the same time, DISTILL-SWAP succeeds until a larger initial age threshold; thus, if the elementary links are of low fidelity to begin with, distilling first might be judicious. Also, in terms of fidelity enhancement (age reduction), DISTILL-SWAP performs better. These conclusions are also consistent with the results in Fig. 18 and 19.

#### Appendix D: Other policies for multiplexing based on SWAP-ASAP

Here we explore multiplexing based SWAP-ASAP policies other than the two paradigmatic versions presented in the main text, namely FN SWAP-ASAP, which prioritizes forming the longest possible links, and SN SWAP-ASAP, which prioritizes forming links with high fidelity. A natural question to ask is how well do policies that are a mixture of these approaches perform. As we have seen that FN outperforms SN in terms of waiting time, but SN outperforms FN in terms of fidelity, the above question is also motivated by the aim to optimize some linear combination of waiting time and fidelity. SN and FN can be mixed in two ways, yielding two different families of policies:

1. *Mixed-weight SWAP-ASAP*: Linear combination of link length and link age can be used to assign the ranks of links for entanglement swapping. Let  $R$  be the metric to decide the rank of a link. Then, a continuous parameter  $a \in [0, 1]$  could be used to define a family of policies as  $R = a|i - j| + (1 - a)m$ , where  $i, j$  are the end-nodes of a link and  $m$  is its age. The limiting cases  $a = 0$  and  $a = 1$  correspond to the SN and FN SWAP-ASAP policies, respectively.
2. *Random-priority SWAP-ASAP*: Keeping the weights to be either the ages of links or their lengths, we could randomly change the priority from SN to FN between different time steps. This would also give a family of policies parameterized by a

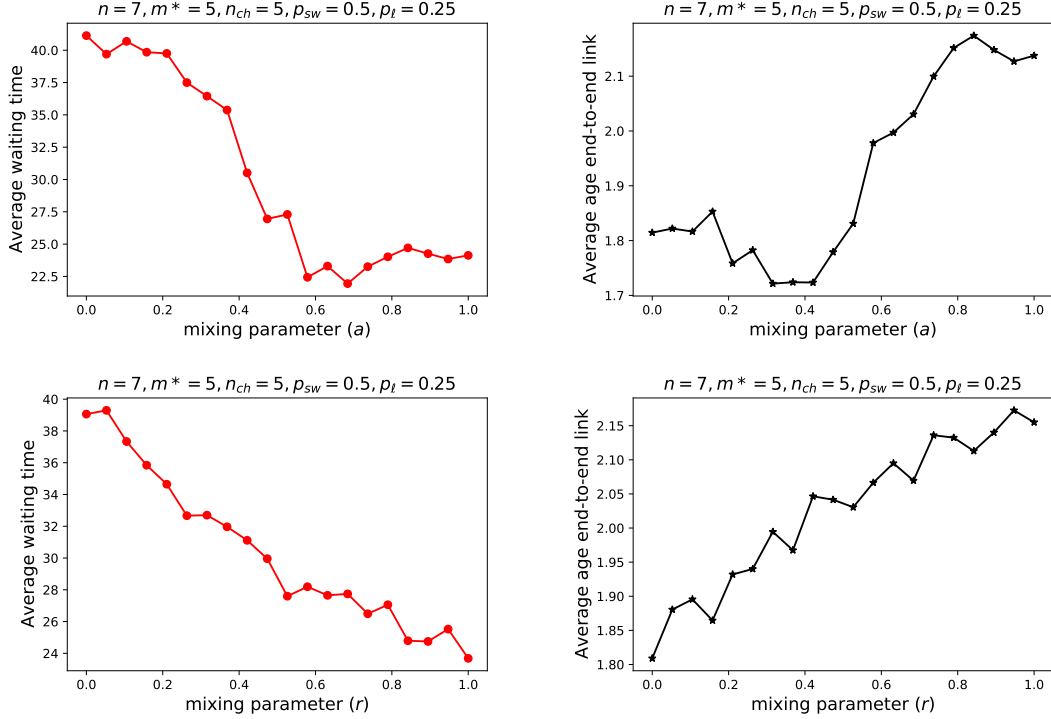


FIG. 21. (Top) Performance of mixed-weight SWAP-ASAP multiplexing policies in terms of average waiting time and age of an end-to-end link, as a function of the mixing parameter  $a$ . FN ( $a = 1$ ) is nearly optimal for waiting time reduction, but a nearly equal mixture of SN and FN ( $a = 0.4$ ) seems to minimize the average age of an end-to-end link. (Bottom) The figures of merit for the random-priority SWAP-ASAP policy show a much more monotonic trend. FN ( $r = 1$ ) is optimal for waiting time and SN ( $r = 0$ ) is optimal for average age.

random number  $r \in [0, 1]$ , which would determine the relative frequencies of choosing the SN and FN policies. Again, we choose  $r$  such that  $r = 0$  and  $r = 1$  would denote the limiting cases, SN and FN, respectively.

Having defined these two families of policies, it is interesting to look at their performance in terms of average waiting time and age of an end-to-end link, as a function of the parameter  $a$ . This is shown in Fig. 21.

Here, we also want to consider the question of optimality of SN and FN SWAP-ASAP in terms of reducing the average age and waiting time for an end-to-end link. Of course, a full optimization could be done by explicitly defining the figure of merit as a cost function and then using tools such reinforcement learning or linear programs to find the optimal entanglement distribution policy within our MDP framework. As was shown in previous works like Refs. [43, 75], the number of MDP states grows exponentially with the number of links and also with the cutoff. Thus, finding the optimal policy explicitly in the multiplexing case is quite challenging, and we leave that as an aim for future work. Here, we ask a limited question. Let us consider a policy that intends to match links for entanglement swapping in such a way that the total length of the virtual links (if entanglement swaps were to be successful) is maximum. We define this policy as *FN optimal*, or FN-OPT policy. In other words, FN-OPT tries all pairings of links for entanglement swapping, calculates the sum of the lengths of the anticipated virtual links, and then chooses the set of pairings that maximizes this sum. Such a pairing could be different from the pairings provided by the usual FN policy, in which the longest link on each side is paired with one another, followed by the second longest, and so on. For example, if we have two links of ages 7 and 3 on each side on a node, then two entanglement swaps can be performed in total. Let us say that the cutoff is 10. The standard FN pairing would be (7, 7) and (3, 3). However, this would mean that the first entanglement swap will never be attempted, because we know that it will fail (as described earlier, the swapped link has age  $m_1 + m_2$ , and we only perform swaps if  $m_1 + m_2 < m^*$ ). Therefore, the sum of lengths of anticipated virtual links in this case will be  $3 + 3 = 6$ . FN-OPT, on the other hand, would choose the pairings (7, 3) and (7, 3), because the sum of anticipated lengths would be  $10 + 10 = 20$ . The intuition for considering FN-OPT is the same as the standard FN policy, i.e., prioritizing forming long links reduces the average waiting time. In a similar way, an *SN-OPT policy* can be defined, which would minimize the sum of the ages of the anticipated links.

In Fig. 22, we compare the performance of FN to FN-OPT and SN to SN-OPT. We can see that the much simpler and standard FN and SN approaches are nearly optimal, in the sense of optimality described above. It is also important to note that the optimal pairings under FN-OPT and SN-OPT will become increasingly complicated to establish with an increasing number of channels, whereas finding the pairings in SN and FN will still remain equally simple.

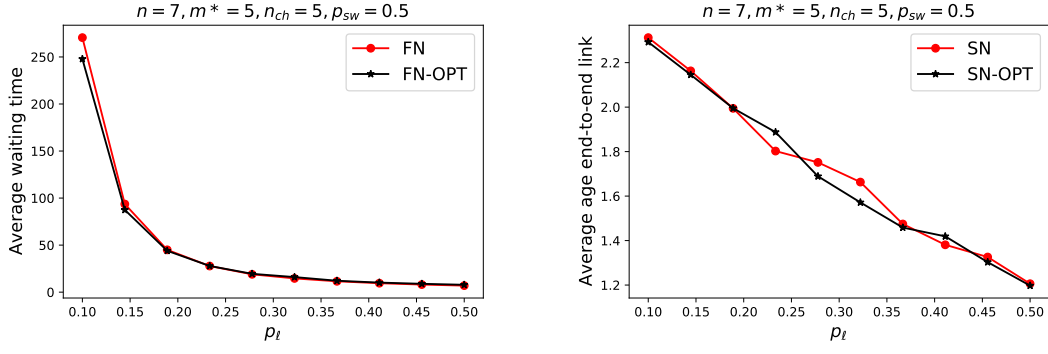


FIG. 22. We compare the performance of FN to FN-OPT and SN to SN-OPT in terms of average waiting time and average age of an end-to-end link. The much simpler and standard FN and SN policies are nearly optimal in both cases.